Available online at www.sciencedirect.com

SCIENCE DIRECT®

PERGAMON

International Journal of Multiphase Flow 29 (2003) 893–926

International Journal of Multiphase Flow

www.elsevier.com/locate/ijmulflow

Deposition of inertia-dominated particles inside a turbulent boundary layer

Mansoo Shin, D.S. Kim, Jin W. Lee *

Department of Mechanical Engineering, Pohang University of Science and Technology, Hyoja 31, Pohang, Kyungbuk 790-784, South Korea

Received 15 October 2001; received in revised form 30 March 2003

Abstract

Non-equilibrium mechanism in the transport of inertia-dominated particles was explained in the problem of particle deposition inside a turbulent boundary layer. Due to the finite inertia of particles and mean shearing of the carrier flows, the transport of inertia-dominated particles inside a turbulent boundary layer is seriously affected by a non-equilibrium memory effect, making the particle retain the memory of its earlier state after spending a characteristic time scale related with the turbulent deposition process. A non-equilibrium constitutive equation for the particle Reynolds stress was derived from the stochastic differential equation of motion of particles governed by the Stokes drag and shear-induced lift forces. This new constitutive model was then applied to the problem of particle deposition in the fully developed turbulent channel flows. It was theoretically predicted that for inertia-dominated particles with $\tau_p^+ > 10$ the distribution of wallward drift velocity in the vicinity of the wall deviates considerably from the equilibrium profile due to an additional turbophoresis, which is generated by the non-equilibrium part of the wall-normal particle Reynolds stress depending on the particle inertia and mean shearing of the carrier flow. And it was also predicted that, when the shear-induced lift force induces a large discrepancy between the particle and fluid motions, the turbulent particle diffusivity might be considerably reduced by the effect of crossing trajectories, resulting in the decrease of diffusive deposition of particles. From this fact it could be postulated that although the shear-induced lift force reduces the diffusive flux of particles, the increase of non-equilibrium wallward drift due to the lift force overwhelms the reduction of diffusive flux and, eventually, enhances the particle deposition to the wall. The predicted deposition velocities as a function of particle relaxation time were in excellent agreement with existing numerical and experimental data.

Keywords: Gas–solid flows; Particle; Turbulent deposition; Particle Reynolds stress; Memory effect; Constitutive equation

* Corresponding author. Tel.: +82-54-279-2170; fax: +82-54-279-3199.
E-mail address: jwlee@postech.ac.kr (J.W. Lee).

0301-9322/03/$ - see front matter © 2003 Elsevier Science Ltd. All rights reserved.
doi:10.1016/S0301-9322(03)00063-6

1. Introduction

The problem of the turbulent deposition of small particles is a representative topic in the area of developing a transport theory of particles. In many cases, to avoid the complications, the researchers has assumed that the suspension of particles is sufficiently dilute so that there is no collision between particles and the particles are not able to modify the surrounding turbulence. Although this one-way coupling problem is much simpler than the two-way coupling, there are still many unsolved problems in the one-way coupled turbulent dispersion in inhomogeneous flows. In an Eulerian description of particle deposition in turbulent flows, the primary transport quantity is the particle flux, J_w, which is usually expressed in the following form:

$$J_w = \left[-\overline{c}\overline{v}_y + (\varepsilon_B + \varepsilon_p)\frac{\partial \overline{c}}{\partial y} \right]_w, \tag{1}$$

where the over-bar denotes a probability–density-weighted average over all possible particle velocities, c the particle concentration (number density), v_y the wall-normal particle velocity, ε_B the particle Brownian diffusivity, and ε_p the particle turbulent diffusivity. The first and the second term on the right-hand side of Eq. (1) represent the convective and the diffusive flux, respectively. And the accuracy of predicted particle deposition or transport depends on the determination of mean particle migration velocity and particle turbulent diffusivity. Both quantities are sensitively dependent on the characteristics of particle fluctuation, which is evidently different from those of the fluid. Such difference between fluid and particle is caused mainly by the inertia of particles, which is usually represented by the particle relaxation time τ_p ($\equiv 1/\beta$) defined by

$$\tau_p^+ = \frac{\rho_p d_p^2}{18\rho_f \nu}\left(\frac{u^{*2}}{\nu}\right), \tag{2}$$

where ρ_p and ρ_f are the material densities of the particle and fluid, respectively, and d_p the particle diameter. The superscript '+' denotes the non-dimensionalization with wall units such as the friction velocity, u^*, and the kinematic viscosity, ν, of the carrier fluid.

Experimental data on the deposition of inertia-dominated particles in turbulent boundary layers, of which mass loading is generally set to be low so as to prevent the particles from modifying the surrounding flow field in most cases, show two distinct features of the effect of particle inertia on the dimensionless deposition velocity V_{dep}^+ defined by

$$V_{dep}^+ = \frac{J_w}{c_m}\left(\frac{1}{u^*}\right), \tag{3}$$

where c_m is the average particle concentration over the cross-sectional area at position x. First, in the diffusion–impaction regime ($1 < \tau_p^+ < 30$), particles acquire an impacting momentum toward the wall through interactions with turbulent eddies, making deposition velocity increase with τ_p^+ dramatically by several orders of magnitude. Second, in the inertia-moderated regime ($\tau_p^+ > 30$), the excessive particle inertia prevents particles from acquiring sufficient impacting momentum from the surrounding turbulent eddies, so that the deposition velocity decreases with τ_p^+. This decline of particle deposition velocity is called the 'roll-off in V_{dep}^+'. These two features are usually

used as the criteria for theoretical models on the transport of particles dispersed in turbulent flows.

The first major deposition model is the stop-distance or free-flight model (Friedlander and Johnstone, 1957; Davies, 1966; Beal, 1968; Liu and Ilori, 1974). In order to match the model predictions with existing experimental data, however, unrealistically high level of fluctuating velocity of the carrier phase need to be used at the local position of a stop distance. Also a large number of arbitrary manipulations were introduced without proper justification. Even with the manipulations it was not explained satisfactorily how particles acquire the necessary wallward momentum from the low level of turbulence at the stop-distance.

Liu and Ilori (1974) recognized that the contradiction in the free-flight model might be caused mainly by the non-equilibrium characteristics of particles with finite inertia, and proposed a new expression for particle turbulent diffusivity, adding a term to account for the enhanced deposition by inertia:

$$\varepsilon_{\mathrm{p}} = \nu_{\mathrm{t}} + \langle u_y'^2 \rangle \tau_{\mathrm{p}}, \tag{4}$$

where ν_{t} is the turbulent eddy viscosity of the carrier turbulence and the angle-bracket denotes the ensemble average over all realizations of the carrier flow. The model yielded a reasonable agreement with experimental data in an intermediate range of particle relaxation time, but not for particles of high inertia. The poor agreement at high inertia is due primarily to the particle diffusivity expression, where ε_{p} increases indefinitely with particle relaxation time and does not reflect the difference between the particle and fluid RMS velocity. Experiments show that particle inertia does not simply manifest itself as an increased diffusivity in the boundary layer (Kallio and Reeks, 1989).

Papavergos and Hedley (1984) supposed that roll-off in V_{dep}^{+} beyond about $\tau_{\mathrm{p}}^{+} = 30$ is mainly due to particle rebound or reentrainment. However, not only theoretical works of Reeks and Skyrme (1976) and Reeks (1982, 1983) but also numerical experiment of Kallio and Reeks (1989) demonstrated that the roll-off in V_{dep}^{+} is directly attributable to the reduction of fluctuating intensity for large particles. This is easily conceivable from the following expression for the wall-normal particle fluctuation in equilibrium with surrounding turbulence (Reeks, 1977),

$$\overline{v_y'^2}(\infty) = \frac{\tau_{\mathrm{L}}}{\tau_{\mathrm{p}} + \tau_{\mathrm{L}}} \langle u_y'^2 \rangle, \tag{5}$$

where τ_{L} is the integral time scale associated with the Lagrangian autocorrelation function of turbulent velocities of the carrier phase and '∞' denotes a local equilibrium. Reeks (1982, 1983) proposed a theory that a particle experiences a force in the direction of decreasing particle fluctuating intensity, and called this mechanism the 'turbophoresis':

$$F_{\mathrm{t}} = -\frac{\mathrm{d}}{\mathrm{d}y} \overline{v_y'^2}. \tag{6}$$

Turbophoresis was shown to induce a wallward particle drift motion, and predictions using a modified gradient-transport concept yielded more reasonable deposition velocity results.

Based on the above equilibrium theory of particle turbulence, Guha (1997) and Young and Leeming (1997) proposed the unified deposition model. Transport equations for the mean particle momentum and concentration were derived in a semi-heuristic way and the second-order

fluctuating moment terms were closed by the constitutive relations based on the traditional Boussinesq hypothesis. For instance, the particle Reynolds shear stress term was closed by applying a simple gradient model based on the Boussinesq hypothesis and the wall-normal stress term by using Eq. (5). The deposition velocity predicted by this model showed a good agreement with experimental measurements over all deposition regimes (diffusional-deposition, diffusion–impaction, and inertia-moderated regimes) in a qualitative sense, but not in the quantitative sense.

As mentioned by Reeks (1993), however, there are so many controversies in closing the particle Reynolds stress using the Boussinesq hypothesis. And it has been pointed out repeatedly that the near-wall profiles of the wall-normal RMS velocity of large particles might be quite different from the profiles computed under the assumption of equilibrium between particles and the local fluid turbulence (Kallio and Reeks, 1989; Kulick et al., 1994; Rouson et al., 1994) and also that it is necessary to consider the non-equilibrium behavior of inertia-dominated particles in the closure of particle Reynolds stress terms in order to predict the inertial deposition of particles more accurately even in a quantitative sense.

Recently, Shin and Lee (2001) proposed the following non-equilibrium constitutive relation for the particle wall-normal stress in fully developed turbulent channel flows, which holds good in the absence of the lift force,

$$\overline{v_y'^2} = \left(1 - \tau_\beta \bar{v}_y \frac{\mathrm{d}}{\mathrm{d}y}\right) \overline{v_y'^2}(\infty), \tag{7}$$

where τ_β denotes a measure of relaxation time scale required to reach a local equilibrium state of the particle Reynolds stress. The relaxation time scale τ_β reflects the dependence of the degree of non-equilibrium on the particle inertia, and is expressed as

$$\tau_\beta \equiv \frac{\mathrm{e}^{-2/St_\tau}}{1 - \mathrm{e}^{-2/St_\tau}} \tau, \tag{8}$$

where St_τ ($\equiv \tau_\mathrm{p}/\tau$) is a Stokes number defined as the ratio of the particle relaxation time, τ_p, to a characteristic time scale for the turbulence–particle interaction in the macroscopic point of view, τ, called an intermediate diffusion time scale (Shin and Lee, 2001). If the particle time scale τ_p becomes comparable to or greater than τ ($St_\tau \gtrsim 1$), the particle Reynolds stress will be in the non-equilibrium state, and a time period τ_β will be required to reach the local equilibrium state given by Eq. (5).

With the introduction of the rather simple non-equilibrium constitutive equation, Shin and Lee (2001) gave much improved predictions for the deposition velocity, showing a good agreement with the Kallio and Reeks' (1989) numerical data for inertia-dominated particles ($\tau_\mathrm{p}^+ > 30$) in the absence of the shear-induced lift force.

For inertia-dominated particles the lift force plays an important role in the deposition process. So this paper is an extension of the authors' preceding work (Shin and Lee, 2001), aiming at a more precise theory for the non-equilibrium particle deposition in fully developed turbulent channel flows. The expression for the particle Reynolds stress is extended to include the effect of shear-induced lift force on the particle motion in an unbounded 2-D simple shear flow. The deposition rates of turbulent particles will be predicted from the particle momentum equation as a function of particle relaxation time both with and without the lift force effect. The prediction results will be compared with the existing numerical and experimental data, and the validity of the

present theory will be tested extensively. Throughout this paper it will be assumed that the particle size and concentration are sufficiently small and low so that there is no collision between particles and the surrounding flow field is not modified by the presence of particles.

2. Governing equations for the particle deposition in a turbulent boundary layer

This section is devoted mainly to a brief summary of the existing unified deposition theory. And also introduced are the slight modifications in the expressions for the particle concentration boundary condition and particle turbulent diffusivity for the inertia-dominated particles. Especially, in the presence of lift force, the particle diffusivity will be modeled to take into account for the effect of relative motion of particles to the fluid on the near-wall distribution of particle diffusivity. Primarily concerned is the flow of solid particles suspended in a fully developed turbulent channel flow. Particles are assumed spherical and mono-dispersed with diameter d_p. It is also assumed that fluid motion is unaffected by the presence of particles and that particle–particle interactions are negligible.

2.1. Particle momentum equations

Mean particle momentum equations in the transverse (y) and streamwise (x) directions for 2-D fully developed turbulent channel flows can be written in dimensionless forms as (Guha, 1997; Young and Leeming, 1997)

$$\bar{v}_y^+ \frac{\mathrm{d}\bar{v}_y^+}{\mathrm{d}y^+} = -\frac{\mathrm{d}}{\mathrm{d}y^+}\overline{v_y'^{+2}} - \frac{Re_p}{24}\frac{C_D}{\tau_p^+}\bar{v}_y^+ + \gamma^+(\langle u_x^+\rangle - \bar{v}_x^+), \tag{9}$$

$$\bar{v}_y^+ \frac{\mathrm{d}\bar{v}_x^+}{\mathrm{d}y^+} = \frac{\mathrm{d}}{\mathrm{d}y^+}\overline{v_x'^+ v_y'^+} + \frac{Re_p}{24}\frac{C_D}{\tau_p^+}(\langle u_x^+\rangle - \bar{v}_x^+), \tag{10}$$

where $Re_p = d_p|\langle \mathbf{u}\rangle - \bar{\mathbf{v}}|/\nu$ is the particle Reynolds number, C_D the particle drag coefficient which is usually given by an empirical correlation in Re_p (see Appendix A), and γ the Saffman lift force coefficient, $\gamma \equiv 3.08(d_p\rho_p/\rho_f)^{-1}(\nu\partial\langle u_x\rangle/\partial y)^{1/2}$.

The second terms on the right-hand side of Eqs. (9) and (10) are the viscous drag terms and the third term in Eq. (9) the lift force term. In order to close the above system of equations, the second-order statistical moment terms, the so-called particle Reynolds stresses, on the right-hand side of Eqs. (9) and (10) have to be modeled by a proper constitutive relationship. Especially, the transverse normal component of the particle Reynolds stress plays an important role in the particle deposition mechanism in such a way that particles acquire a drift velocity in the direction of decreased fluctuation intensity. In general, an accurate representation of these terms are difficult because particle turbulence properties are different from those of carrier flow due to particle inertia and particle drift relative to the surrounding fluid. Inside the turbulent boundary layers, inertia-dominated particles may drift into regions of quite different turbulence levels while retaining a partial memory of their earlier motion, part of the mean and fluctuating velocities at previous times. This is called 'the non-equilibrium memory effect'. In all the previous studies this memory effect was ignored, and it has been assumed that the fluctuating intensity of the particles

Table 1
Existing constitutive equations

	Transverse normal component, $\overline{v_y'^2}$	Shear component, $\overline{v_x'v_y'}$
Guha (1997); Young and Leeming (1997)	$\frac{\tau_L}{\tau_p+\tau_L}\langle u_y'^2\rangle$	$-\nu_t\frac{d\bar{v}_x}{dy}$
Shin and Lee (2001)	$\left(1-\tau_\beta\bar{v}_y\frac{d}{dy}\right)\frac{\tau_L}{\tau_p+\tau_L}\langle u_y'^2\rangle$	$-\nu_t\frac{d\bar{v}_x}{dy}$

depends only on the local value of fluctuating intensity of the surrounding fluid turbulence just as if particles were always in equilibrium in a homogeneous turbulent flow. Shin and Lee (2001) proposed the first non-equilibrium constitutive relation in a form given in Eq. (7). $\overline{v_x'v_y'}$ was modeled by a gradient diffusion model with turbulent eddy viscosity equal to that of the carrier phase. Briefly summarized in Table 1 are the existing constitutive equations for $\overline{v_y'^2}$ and $\overline{v_x'v_y'}$. In Section 3, improved non-equilibrium constitutive equations will be formulated with the lift force effect included.

2.2. Particle concentration equation

In the fully developed conditions, the concentration profile and the particle mass flux can be normalized by the mean concentration, and the normalized profiles become independent of x^+:

$$\phi(y^+)=\frac{\bar{c}(x^+,y^+)}{c_m(x^+)}. \tag{11}$$

The normalized concentration equation and the boundary conditions can be expressed as (Young and Leeming, 1997)

$$-\kappa\bar{v}_x^+\phi+\frac{d}{dy^+}\bar{v}_y^+\phi=\frac{d}{dy^+}\left[(\varepsilon_B^+ +\varepsilon_p^+)\frac{d\phi}{dy^+}\right], \tag{12}$$

$$V_{dep}^+\equiv\left[-\bar{v}_y^+\phi+(\varepsilon_B^+ +\varepsilon_p^+)\frac{d\phi}{dy^+}\right]_{y^+=d_p^+/2}=\left[\frac{1}{2}\bar{v}_y^+\phi\left\{\frac{1}{\sqrt{\pi}\xi}e^{-\xi^2}-\mathrm{erfc}(\xi)\right\}\right]_{y^+=d_p^+/2}, \tag{13}$$

$$\left.\frac{d\phi}{dy^+}\right|_{y^+=h^+}=0, \tag{14}$$

where κ is a constant related with the deposition velocity,

$$\kappa\equiv\frac{V_{dep}^+}{\langle\bar{v}_x^+\rangle_\phi} \tag{15}$$

in which $\langle\cdot\rangle_\phi$ denotes a weighted average based on the normalized concentration profile ϕ over the domain of $d_p/2<y<h$. In Eq. (12) $\varepsilon_B=R_pT_p\tau_p$ and $R_p=k_B/m_p$, where k_B is the Boltzmann constant and $m_p=\pi d_p^3\rho_p/6$ the particle mass. Since ε_B is inversely proportional to particle diameter, it becomes smaller and smaller than ε_p as the particle size increases.

Though the basic equations (12) and (13) are correct, the choice of ξ in Eq. (13) needs to be modified. Eq. (13) is the near-wall boundary condition which was derived originally by Young

and Leeming (1997) from a simple kinetic approach based on a Maxwellian distribution of particle velocity, with a mean of $\bar{v}_y$ and a variance of R_pT:

$$\xi = \bar{v}_y/\sqrt{2R_pT}. \tag{16}$$

This boundary condition is justified only when the particle fluctuation comes from thermal fluctuation alone. However, the wall boundary condition is actually applied at a distance of one particle radius from the wall, where the turbulence intensity is not zero. So it is necessary to modify the boundary condition given in Eq. (16) in such a way that particle fluctuation due to turbulent flow as well as thermal fluctuation is considered in the definition of the variance. These two different fluctuations may occur with quite different time scales from each other, so that their fluctuating motions can be assumed statistically independent of each other. Furthermore, if we simply assume the Gaussian distribution of particle fluctuating velocities in the near-wall region for the lack of any better information, the variance of particle velocity can be rewritten as

$$\sigma^2 = R_pT + \overline{v_y'^2}. \tag{17}$$

Now ξ defined in Eq. (16) is changed into

$$\xi = \bar{v}_y \Big/ \sqrt{2(R_pT + \overline{v_y'^2})}. \tag{18}$$

This correction has an important meaning in the mechanism of turbulent particle deposition. The non-equilibrium ξ in Eq. (18) is always smaller than the equilibrium ξ in Eq. (16), and Eq. (13) shows that the non-equilibrium deposition velocity always becomes larger than the equilibrium deposition velocity. So this correction partially explains the finding that the non-equilibrium memory effect enhances particle deposition through the enhanced fluctuating intensity of particles in the near-wall region (Shin and Lee, 2001).

2.3. Model of particle turbulent diffusivity

It has been assumed extensively that, inside the fully developed turbulent boundary layers, the particle diffusivity is equal to the turbulent eddy viscosity of the carrier phase (Friedlander and Johnstone, 1957; Guha, 1997; Young and Leeming, 1997; Shin and Lee, 2001):

$$\varepsilon_p = \nu_t. \tag{19}$$

This assumption is valid when particle motion deviates only a little bit from fluid motion. When the particle drift relative to the fluid is large, the particle diffusivity can be much different from ν_t by the effect of crossing trajectories, which is the case for large particles in the near wall region. Inside the turbulent boundary layer, the inclusion of shear-induced lift force in the particle equation of motion brings about a considerably large relative motion of inertia-dominated particles to the carrier fluid. For this reason, the simple modification of ε_p is considered for the case of the inclusion of lift force, in such a way that ε_p probably becomes smaller than ν_t due to 'the effect of crossing trajectories'.

Unfortunately it is difficult to analyze the turbulent dispersion of particles in the presence of mean relative drift even for simple turbulence conditions, and most of the models for the dispersion of turbulent particles and the particle diffusivity have been derived through ad hoc

assumptions (Tchen, 1947; Friedlander, 1957; Csanady, 1963; Chao, 1964; Peskin, 1971; Meek and Jones, 1974; Reeks, 1977). Following the dispersion theory of Csanady (1963), the particle turbulent diffusivity in the presence of the crossing trajectory effect can be expressed as

$$\tilde{\varepsilon}_{\mathrm{p}} = v_{\mathrm{t}} \left[1 + \left(\frac{l_{\mathrm{L}}}{l_{\mathrm{E}}} \frac{\Delta v}{\sqrt{\overline{v_y'^2}}} \right)^2 \right]^{-1/2}, \tag{20}$$

where $\Delta v \equiv |\bar{\mathbf{v}} - \langle \mathbf{u} \rangle|$ is the particle drift velocity relative to the surrounding fluid. l_{L} and l_{E} denote the Lagrangian integral length scale and the Eulerian length scale of the flow turbulence, respectively, usually obtained from the following relationships (Hinze, 1975):

$$l_{\mathrm{L}} \equiv \langle u_y'^2 \rangle^{1/2} \tau_{\mathrm{L}}, \tag{21}$$

$$l_{\mathrm{E}} \equiv 1.25 l_{\mathrm{L}}. \tag{22}$$

Eq. (20) is coupled with the particle momentum equation because the drift velocity and the particle RMS velocity are implicitly dependent on $\tilde{\varepsilon}_{\mathrm{p}}$. In order to simplify the problem, it is assumed here that the particle fluctuations are in equilibrium with the surrounding turbulence, which is assumed to be locally homogeneous and stationary. Then the $\tilde{\varepsilon}_{\mathrm{p}}$ can be finally expressed as

$$\tilde{\varepsilon}_{\mathrm{p}} = v_{\mathrm{t}} \left[1 + \frac{\tau_{\mathrm{p}} + \tau_{\mathrm{L}}}{\tau_{\mathrm{L}}} \left(\frac{l_{\mathrm{L}}}{l_{\mathrm{E}}} \frac{\Delta v}{\sqrt{\langle u_y'^2 \rangle}} \right)^2 \right]^{-1/2}. \tag{23}$$

Eq. (23) implies that, as the particle inertia and the particle drift velocity increase, the particle diffusivity decreases due to the effect of crossing trajectories.

3. Non-equilibrium closure of the particle Reynolds stress

3.1. Constitutive equation for the particle Reynolds stress

When solid particles are dilutely suspended in turbulent shear flows and their motion is governed mainly by both the Stokes drag and the shear-induced lift force (Saffman, 1965), the equation of motion in the form of Langevin equation can be written as

$$\frac{\mathrm{d}\mathbf{v}}{\mathrm{d}t} = -\mathbf{B} \cdot \mathbf{v} + \langle \mathbf{f} \rangle + \mathbf{f}', \tag{24}$$

where $\langle \mathbf{f} \rangle$ and $\mathbf{f}'$ denote the mean and the fluctuating aerodynamic forces acting on the particle along its trajectory, respectively. As a good approximation, these forces can be expressed as

$$\langle \mathbf{f} \rangle = \mathbf{B} \cdot \langle \mathbf{u} \rangle, \tag{25}$$

$$\mathbf{f}' = \mathbf{B} \cdot \mathbf{u}'. \tag{26}$$

The components of the friction coefficient tensor $\mathbf{B}$ can be written as

$$B_{ij} = \beta\delta_{ij} + \gamma_{ij}, \tag{27}$$

where δ_{ij} is the Kronecker delta tensor. β and γ_{ij} are the Stokes drag and Saffman lift coefficients, respectively, and are usually defined as follows:

$$\beta = \frac{18\nu}{Sd_{\mathrm{p}}^2}, \tag{28}$$

$$\gamma_{ij} = \frac{k\sqrt{\nu}}{Sd_{\mathrm{p}}(\mathbf{d}_{\mathrm{f}} : \mathbf{d}_{\mathrm{f}})^{1/4}} d_{\mathrm{f},ij}, \tag{29}$$

where $k = 2.594$, S the density ratio of solid particle to carrier fluid and $d_{\mathrm{f},ij}$ the coefficient of deformation tensor of the fluid flow. The deformation tensor is again defined as

$$\mathbf{d}_{\mathrm{f}} = \frac{1}{2}(\mathbf{s}_{\mathrm{f}} + \mathbf{s}_{\mathrm{f}}^{\mathrm{T}}), \tag{30}$$

where the superscript 'T' indicates the transpose of tensor and $\mathbf{s}_{\mathrm{f}}$ the shear rate tensor whose components are defined as

$$s_{\mathrm{f},ij} \equiv \partial\langle u_i\rangle/\partial x_j. \tag{31}$$

Now the Langevin equation of motion for the particles is stochastically averaged and the results are expressed in terms of the following statistical moments (Reeks, 1993):

$$\mu_{ij} \equiv \langle v_i f_j'\rangle, \tag{32}$$

$$\lambda_{ij} \equiv \langle x_i f_j'\rangle, \tag{33}$$

$$\varepsilon_{ij} \equiv \langle v_i' x_j'\rangle \cong B_{ik}^{-1}(\overline{v_k' v_j'} + \lambda_{jk}), \tag{34}$$

where μ_{ij}, λ_{ij} and ε_{ij} are defined from the fluid-to-particle interactions along the particle trajectories. Then the long-time equilibrium particle Reynolds stress is obtained as follows:

$$\overline{v_i v_j}(\infty) = \frac{1}{2\beta}(\Theta_{ij} + \Theta_{ji})(\infty), \tag{35}$$

$$\Theta_{ij} \equiv \mu_{ij} + \gamma_{ik}\lambda_{kj} + [(\beta\delta_{ik} + \gamma_{ik})(s_{\mathrm{p},kl} - s_{\mathrm{f},kl}) - s_{\mathrm{p},ik}s_{\mathrm{p},kl}]\varepsilon_{jl} - (s_{\mathrm{p},ik} + \gamma_{ik})\varepsilon_{lk}(\beta\delta_{jl} + \gamma_{jl}), \tag{36}$$

where the components of the particle shear rate tensor, $s_{\mathrm{p},ij}$, is defined by

$$s_{\mathrm{p},ij} \equiv \partial\bar{v}_i/\partial x_j. \tag{37}$$

For the condition of simple shear flows (see Fig. 1), the flow field can be written as follows:

$$\langle \mathbf{u}\rangle = s_{\mathrm{f},xy} y\mathbf{i} + 0\mathbf{j}, \tag{38}$$

$$\bar{\mathbf{v}} \approx s_{\mathrm{p},xy} y\mathbf{i} + s_{\mathrm{p},yy} y\mathbf{j}. \tag{39}$$

If it is assumed that flow turbulence is locally homogeneous and the shear-induced lift force acts only in the transverse direction (γ_{11}, γ_{12}, $\gamma_{22} = 0$, $\gamma_{21} = \gamma$), the transverse normal and shear components of the long-time particle Reynolds stress are expressed as follows, respectively:

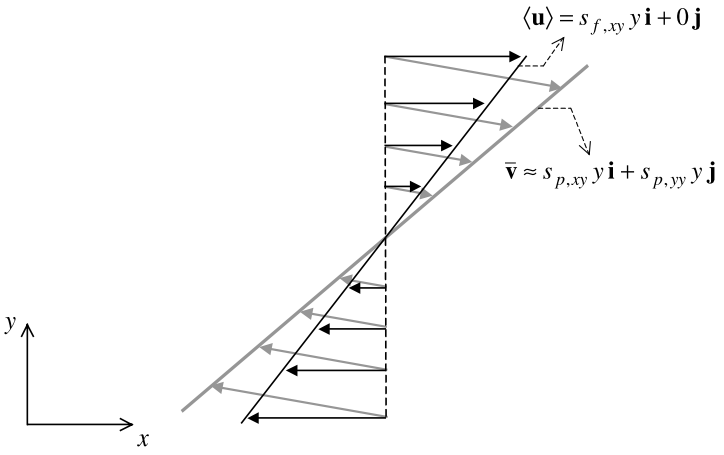

Fig. 1. Schematic of the mean velocity field in the 2-D simple shear flow.

$$\overline{v_y'^2}(\infty) = \frac{1}{\beta}\mu_{yy}(\infty) + \frac{\gamma}{\beta}\lambda_{xy}(\infty) - \frac{\gamma^2}{\beta}\varepsilon_{xx}(\infty) - \gamma\varepsilon_{yx}(\infty) + \frac{\gamma}{\beta}(s_{\mathrm{f},xy} - s_{\mathrm{p},xy})\varepsilon_{yy}(\infty) - \left[\frac{\gamma}{\beta}\varepsilon_{xy}(\infty) + 2\varepsilon_{yy}(\infty)\right]s_{\mathrm{p},yy} - \frac{1}{\beta}\varepsilon_{22}(\infty)s_{\mathrm{p},yy}^2, \tag{40}$$

$$\overline{v_x'v_y'}(\infty) = \frac{1}{2\beta}(\mu_{xy} + \mu_{yx})(\infty) + \frac{\gamma}{2\beta}\lambda_{xx}(\infty) - \frac{\gamma}{2}\varepsilon_{xx}(\infty) + \left[\frac{\gamma}{2\beta}\varepsilon_{xy}(\infty) + \frac{1}{2}\varepsilon_{yy}(\infty)\right]s_{\mathrm{f},xy} - \left[\frac{\gamma}{\beta}\varepsilon_{xy}(\infty) + \varepsilon_{yy}(\infty)\right]s_{\mathrm{p},xy}. \tag{41}$$

Detailed derivation of the limiting forms of the dispersion coefficients, μ_{yy}, μ_{xy}, μ_{yx}, λ_{xy}, and λ_{xx}, are given in Appendix A and the final resulting expressions are as follows:

$$\mu_{xy}(\infty) = \varepsilon_{xx}^0\beta\gamma\frac{1+\beta\tau_{\mathrm{L},xx} - \gamma s_{\mathrm{f}}\tau_{\mathrm{L},xx}^2}{(1+\beta\tau_{\mathrm{L},xx})^2 - \gamma s_{\mathrm{f}}\tau_{\mathrm{L},xx}^2} + \varepsilon_{xy}^0\beta^2\frac{1+\beta\tau_{\mathrm{L},xy} - \gamma s_{\mathrm{f}}\tau_{\mathrm{L},xy}^2}{(1+\beta\tau_{\mathrm{L},xy})^2 - \gamma s_{\mathrm{f}}\tau_{\mathrm{L},xy}^2} + \varepsilon_{xx}^0\frac{s_{\mathrm{f}}\gamma^2\beta\tau_{\mathrm{L},xx}^2}{(1+\beta\tau_{\mathrm{L},xx})^2 - \gamma s_{\mathrm{f}}\tau_{\mathrm{L},xx}^2} + 2\varepsilon_{xy}^0\frac{s_{\mathrm{f}}\gamma\beta^2\tau_{\mathrm{L},xy}^2}{(1+\beta\tau_{\mathrm{L},xy})^2 - \gamma s_{\mathrm{f}}\tau_{\mathrm{L},xy}^2} + \varepsilon_{yy}^0\frac{s_{\mathrm{f}}\beta^3\tau_{\mathrm{L},yy}^2}{(1+\beta\tau_{\mathrm{L},yy})^2 - \gamma s_{\mathrm{f}}\tau_{\mathrm{L},yy}^2}, \tag{42}$$

$$\mu_{yx}(\infty) = \varepsilon_{xx}^0\frac{\beta^2\gamma\tau_{\mathrm{L},xx}}{\gamma s_{\mathrm{f}}\tau_{\mathrm{L},xx}^2 - (1+\beta\tau_{\mathrm{L},xx})^2} + \varepsilon_{xx}^0\beta\gamma\frac{1+\beta\tau_{\mathrm{L},xx}}{(1+\beta\tau_{\mathrm{L},xx})^2 - \gamma s_{\mathrm{f}}\tau_{\mathrm{L},xx}^2} + \varepsilon_{yx}^0\beta^2\frac{1+\beta\tau_{\mathrm{L},yx}}{(1+\beta\tau_{\mathrm{L},yx})^2 - \gamma s_{\mathrm{f}}\tau_{\mathrm{L},yx}^2}, \tag{43}$$

$$\mu_{yy}(\infty) = \varepsilon^0_{xx}\frac{\gamma^2\beta\tau_{\mathrm{L},xx}}{\gamma s_\mathrm{f}\tau^2_{\mathrm{L},xx} - (1+\beta\tau_{\mathrm{L},xx})^2} + \varepsilon^0_{xy}\frac{\gamma\beta^2\tau_{\mathrm{L},xy}}{\gamma s_\mathrm{f}\tau^2_{\mathrm{L},xy} - (1+\beta\tau_{\mathrm{L},xy})^2} + \varepsilon^0_{xx}\gamma^2\frac{1+\beta\tau_{\mathrm{L},xx}}{(1+\beta\tau_{\mathrm{L},xx})^2 - \gamma s_\mathrm{f}\tau^2_{\mathrm{L},xx}} + 2\varepsilon^0_{xy}\beta\gamma\frac{1+\beta\tau_{\mathrm{L},xy}}{(1+\beta\tau_{\mathrm{L},xy})^2 - \gamma s_\mathrm{f}\tau^2_{\mathrm{L},xy}} + \varepsilon^0_{yy}\beta^2\frac{1+\beta\tau_{\mathrm{L},yy}}{(1+\beta\tau_{\mathrm{L},yy})^2 - \gamma s_\mathrm{f}\tau^2_{\mathrm{L},yy}}, \tag{44}$$

$$\lambda_{xx}(\infty) = \beta^2\varepsilon^0_{xx}\frac{(1+\beta\tau_{\mathrm{L},xx})\tau_{\mathrm{L},xx} - \gamma s_\mathrm{f}\tau^3_{\mathrm{L},xx}}{(1+\beta\tau_{\mathrm{L},xx})^2 - \gamma s_\mathrm{f}\tau^2_{\mathrm{L},xx}} + \varepsilon^0_{xx}\frac{s_\mathrm{f}\gamma\beta^2\tau^3_{\mathrm{L},xx}}{(1+\beta\tau_{\mathrm{L},xx})^2 - \gamma s_\mathrm{f}\tau^2_{\mathrm{L},xx}} + \varepsilon^0_{yx}\frac{s_\mathrm{f}\beta^3\tau^3_{\mathrm{L},yx}}{(1+\beta\tau_{\mathrm{L},yx})^2 - \gamma s_\mathrm{f}\tau^2_{\mathrm{L},yx}}, \tag{45}$$

$$\lambda_{xy}(\infty) = \varepsilon^0_{xx}\beta\gamma\frac{(1+\beta\tau_{\mathrm{L},xx})\tau_{\mathrm{L},xx} - \gamma s_\mathrm{f}\tau^3_{\mathrm{L},xx}}{(1+\beta\tau_{\mathrm{L},xx})^2 - \gamma s_\mathrm{f}\tau^2_{\mathrm{L},xx}} + \varepsilon^0_{xy}\beta^2\frac{(1+\beta\tau_{\mathrm{L},xy})\tau_{\mathrm{L},xy} - \gamma s_\mathrm{f}\tau^3_{\mathrm{L},xy}}{(1+\beta\tau_{\mathrm{L},xy})^2 - \gamma s_\mathrm{f}\tau^2_{\mathrm{L},xy}} + \varepsilon^0_{xx}\frac{s_\mathrm{f}\gamma^2\beta\tau^3_{\mathrm{L},xx}}{(1+\beta\tau_{\mathrm{L},xx})^2 - \gamma s_\mathrm{f}\tau^2_{\mathrm{L},xx}} + 2\varepsilon^0_{xy}\frac{s_\mathrm{f}\gamma\beta^2\tau^3_{\mathrm{L},xy}}{(1+\beta\tau_{\mathrm{L},xy})^2 - \gamma s_\mathrm{f}\tau^2_{\mathrm{L},xy}} + \varepsilon^0_{yy}\frac{s_\mathrm{f}\beta^3\tau^3_{\mathrm{L},yy}}{(1+\beta\tau_{\mathrm{L},yy})^2 - \gamma s_\mathrm{f}\tau^2_{\mathrm{L},yy}}. \tag{46}$$

The particle diffusivity in the long-time limit, $\varepsilon_{ij}(\infty)$, in Eqs. (40) and (41) was assumed equal to that of the flow, which was assumed locally homogeneous stationary, as a good approximation (Reeks, 1977; Pismen and Nir, 1978):

$$\varepsilon_{ij}(\infty) = \varepsilon^0_{ij} \equiv \tau_\mathrm{L}\langle u'_i u'_j\rangle. \tag{47}$$

Since the wall-normal particle fluctuation is the predominant factor in the deposition process and the inclusion of lift force may not generate an appreciable amount of memory effect in the shear component, the non-equilibrium constitutive relation is applied to the transverse normal component of the particle Reynolds stress only. In Eq. (40) $s^2_{\mathrm{p},yy}$ can be safely neglected because the magnitude of $s_{\mathrm{p},yy}$ is usually much smaller than those of $s_{\mathrm{p},xy}$ and $s_{\mathrm{f},xy}$. If it is further assumed that the y-directional derivative of this gradient diffusion term is negligible, the constitutive relations for the particle Reynolds stress become

$$\overline{v'^2_y} = -D_{yy}\frac{\mathrm{d}\bar{v}_y}{\mathrm{d}y} + \left(1 - \tau_\beta\bar{v}_y\frac{\mathrm{d}}{\mathrm{d}y}\right)\varsigma_{yy}, \tag{48}$$

$$\overline{v'_x v'_y} = -D_{xy}\frac{\mathrm{d}\bar{v}_x}{\mathrm{d}y} + \varsigma_{xy}, \tag{49}$$

where coefficients D_{xy}, D_{yy}, ζ_{xy} and ζ_{yy} are defined as

$$D_{yy} \equiv \frac{\gamma}{\beta}\varepsilon_{xy}(\infty) + 2\varepsilon_{yy}(\infty), \tag{50}$$

$$D_{xy} \equiv \frac{\gamma}{\beta}\varepsilon_{xy}(\infty) + \varepsilon_{yy}(\infty), \tag{51}$$

$$\varsigma_{yy} \equiv \frac{1}{\beta}\mu_{yy} + \frac{\gamma}{\beta}\lambda_{xy} - \frac{\gamma^2}{\beta}\varepsilon_{xx} - \gamma\varepsilon_{yx} + \frac{\gamma}{\beta}\varepsilon_{yy}(s_{\mathrm{f},xy} - s_{\mathrm{p},xy}), \tag{52}$$

$$\varsigma_{xy} \equiv \frac{1}{2\beta}(\mu_{xy} + \mu_{yx}) + \frac{\gamma}{2\beta}\lambda_{xx} - \frac{\gamma}{2}\varepsilon_{xx} + \frac{1}{2}\left(\frac{\gamma}{\beta}\varepsilon_{xy} + \varepsilon_{yy}\right)s_{\mathrm{f},xy}. \tag{53}$$

In contrast to the traditional simple gradient models, the present relationship for $\overline{v'_x v'_y}$ includes an additional term ζ_{xy} besides the gradient diffusion term. Through this term, $\overline{v'_x v'_y}$ depends not only on the spatial gradient of $\bar{v}_x$, but also on the particle inertia and the mean shear rate and turbulence level of the flow.

Throughout all the calculations, the diffusion coefficients of the flow in Eqs. (50)–(53) are assumed equal to those for the locally isotropic turbulence of the flow; that is, $\varepsilon^0_{xy}, \varepsilon^0_{yx} = 0$, and $\varepsilon^0_{xx} = \varepsilon^0_{yy} = \nu_{\mathrm{t}}$. And it is also assumed that $\tau_{\mathrm{L},ij} = \tau_{\mathrm{L}}$ for all $i, j = x$ or y.

3.2. Choice of the intermediate diffusion time scale, τ

As is clear from Eqs. (7) and (48), the amount of correction for the memory effect is sensitively dependent on the intermediate diffusion time scale τ, and τ has to be chosen depending on the characteristic time scale of the mechanism of interest. For the problem of particle deposition in a fully developed turbulent channel flow, the characteristic scale of turbulent eddies in the vicinity of the wall may be the best candidate for the characteristic scale of the deposition process. And the Lagrangian integral time scale of turbulence is generally the most representative time scale of turbulent eddy motion. Thus, it is most reasonable to choose the Lagrangian integral time scale close to the wall as τ. Measurements of organized near-wall structures have indicated that the time scale is approximately constant at $\tau^+_{\mathrm{L}} \approx 10$ in the near-wall region (Wallace et al., 1972; Brodkey et al., 1974; Luchik and Tiederman, 1987), and τ is expected to be close to this value.

As a criterion for the choice of τ, deposition velocities are calculated for values of τ^+ ranging from 0.1 to 1000 (see Fig. 2), using the simple non-equilibrium model (Shin and Lee, 2001) in the absence of the lift force. As can be seen in Fig. 2, the deposition curves move only within a rather limited range with the variation of τ^+ and the estimated deposition curve approaches the equilibrium curve as τ^+ goes to infinity. Kallio and Reeks' (1989) Lagrangian particle tracking data for $\tau^+_{\mathrm{p}} = 30$ and 100 imply that τ^+ coincides roughly with the Lagrangian integral time scale estimated in the experiments of organized near-wall structures ($\tau^+_{\mathrm{L}} \approx 10$). In the present work, $\tau^+ = 5$ will be used throughout all the calculations of turbulent particle deposition. If a much larger τ^+ than the characteristic time scale of the near-wall turbulent eddies is used, the detailed information of particle–eddy interaction will be lost, and the predicted deposition rate will approach the equilibrium value with increased τ^+.

3.3. Summary of the present model for the constitutive equations

In this chapter, we derived the long-time values of $\overline{v'^2_y}$ and $\overline{v'_x v'_y}$ in the presence of shear-induced lift force under the assumption that the surrounding turbulence is locally homogeneous. The only

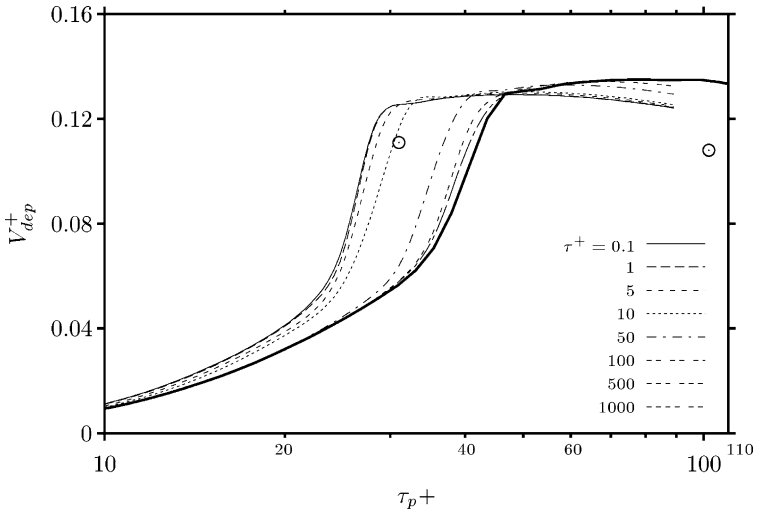

Fig. 2. Variation of $V^+_{\mathrm{dep}}(\tau^+_{\mathrm{p}})$ with τ^+ in the absence of the lift force: thin lines, Shin and Lee (2001) model; solid thick line, equilibrium model; ⊙, Kallio and Reeks (1989).

Table 2
Comparison between constitutive equations

	Transverse normal component, $\overline{v_y'^2}$	Shear component, $\overline{v_x' v_y'}$
Guha (1997); Young and Leeming (1997)	$\frac{\tau_{\mathrm{L}}}{\tau_{\mathrm{p}}+\tau_{\mathrm{L}}}\langle u_y'^2\rangle$	$-\nu_{\mathrm{t}}\frac{\mathrm{d}\bar{v}_y}{\mathrm{d}y}$
Shin and Lee (2001)	$\left(1-\tau_\beta \bar{v}_y \frac{\mathrm{d}}{\mathrm{d}y}\right)\frac{\tau_{\mathrm{L}}}{\tau_{\mathrm{p}}+\tau_{\mathrm{L}}}\langle u_y'^2\rangle$	$-\nu_{\mathrm{t}}\frac{\mathrm{d}\bar{v}_y}{\mathrm{d}y}$
Present	$-D_{yy}\frac{\mathrm{d}\bar{v}_y}{\mathrm{d}y}+\left(1-\tau_\beta \bar{v}_y \frac{\mathrm{d}}{\mathrm{d}y}\right)\zeta_{yy}$	$-D_{xy}\frac{\mathrm{d}\bar{v}_y}{\mathrm{d}y}+\zeta_{xy}$

stringent assumption used is that the long-time particle turbulent diffusivity is equal to that of the fluid so it is independent of the mean shear rate of the flow. The adoption of this assumption is rather inevitable either due to the lack of any better information or to limit the complexity of the formulas to a proper level.

Table 2 briefly summarizes the comparison of important terms in the non-equilibrium constitutive equations for the turbulent deposition of particles between the present model and the existing ones.

4. Results and discussion

The set of equations (9), (10) and (12) are solved numerically using the pseudo-transient iteration method. The equations are discretized using the finite volume method and the upwind scheme is applied to the convective terms. Simulation conditions are summarized in Table 3, and surrounding turbulence quantities are specified by (A.1)–(A.9).

Table 3
Simulation conditions

$Re\ (\equiv U_c h/\nu)$	h^+	ν	u^*	ρ_f	ρ_p/ρ_f
3300	180	1.502×10^{-5} m^2/s	5.45×10^{-2} m/s	1.205 kg/m^3	713

4.1. Non-equilibrium wall-normal particle RMS velocity

The particle momentum transport toward the wall inside the turbulent boundary layer is most strongly affected by $\overline{v_y'^2}$ through the turbophoresis term in the momentum equation (9). Also $\overline{v_y'^2}$ influences the gradient of particle concentration through the boundary condition (13). According to Eq. (13), the gradient of particle concentration depends on the parameter which is the ratio of $\bar{v}_y$ to $\sqrt{\overline{v_y'^2}}$ in the vicinity of the wall, in such a way that when the particle mean velocity becomes much greater than the particle RMS velocity ($\xi \gg 1$) the gradient of particle concentration approaches 0. Judging from these facts, an accurate prediction of $\overline{v_y'^2}$ is directly connected to an accurate prediction of the inertial deposition of large particles.

Near-wall distributions of particle RMS velocity for various particle relaxation times are predicted by the present non-equilibrium theory, and they are compared with predictions by the equilibrium theory in Fig. 3(a) and (b). In order to compare the predictions with DNS results of Rouson et al. (1994), particles with $\tau_p^+ = 9, 117, 810$ are considered. Fig. 3(a) compares the DNS results with the predictions in the absence of the shear-induced lift force ($\gamma = 0$) and Fig. 3(b) in the presence of the lift force ($\gamma \neq 0$). In the turbulence-core region ($y^+ > 30$), where the flow turbulence is almost homogeneous, both the present equilibrium theory and the non-equilibrium theory give almost the same prediction about the reduction of particle turbulence intensity with particle relaxation time. In the near-wall region ($y^+ < 30$), on the other hand, the predictions by the present theory deviate from those by the equilibrium theory. This discrepancy becomes larger with increased τ_p^+. It can be attributed to the memory effect of inertia-dominated particles by which particles retain a high level of fluctuating intensity as they travel from the turbulence-core region into the near-wall region. For the particles with $\tau_p^+ = 117$ and 810, there exist striking differences between the non-equilibrium and the equilibrium distributions. In the near-wall region, the predicted non-equilibrium RMS velocities are in much better agreement with DNS results compared with those computed under the local equilibrium assumption (Fig. 3(a)).

Inclusion of the shear-induced lift force in the particle momentum equation increases the wallward particle velocity in the strong shear region ($y^+ < 30$), and makes the large particles maintain their high level of fluctuating intensity much closer to the wall than in the absence of the lift force (Fig. 3(b)). The lift force has an effect of increasing the particle fluctuating intensity in the near-wall region, and, as will be mentioned later, the concentration profiles of large particles become flatter in the vicinity of the wall by the lift force.

Plotted in Fig. 4(a) and (b) is the predicted additional RMS velocities induced from the non-equilibrium factors, such as the inhomogeneity of boundary layer turbulence and particle inertia, for various particle relaxation times. It is clearly shown that, inside the strong shear region ($y^+ < 30$), the RMS velocities of large particles are higher than the values predicted under the local equilibrium assumption and the discrepancy becomes larger with increasing the particle

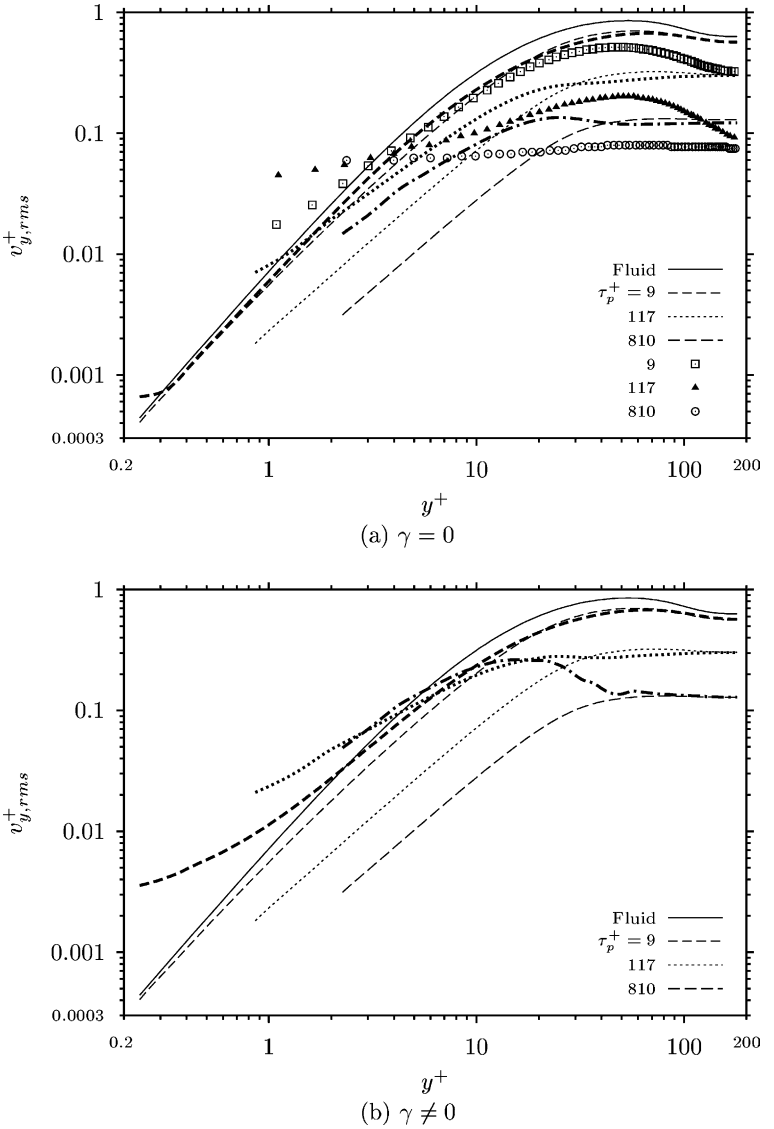

Fig. 3. Distribution of $v^+_{y,\mathrm{rms}}$ in the boundary layer (a) without and (b) with the lift force: thin lines, equilibrium model; thick lines, non-equilibrium model. DNS data from Rouson et al. (1994): ⊡, 28 μm lycopodium ($\tau_\mathrm{p}^+ = 9$); ▲, 50 μm glass ($\tau_\mathrm{p}^+ = 117$); ⊙, 70 μm copper ($\tau_\mathrm{p}^+ = 810$).

inertia. It is also seen that the shear-induced lift force augments the non-equilibrium increment of RMS velocity with particle inertia.

4.2. Non-equilibrium turbophoresis

The wall-normal gradient of particle fluctuating velocity inside the boundary layer induces a force to accelerate particles toward the wall, and the force is called turbophoresis (Reeks, 1983),

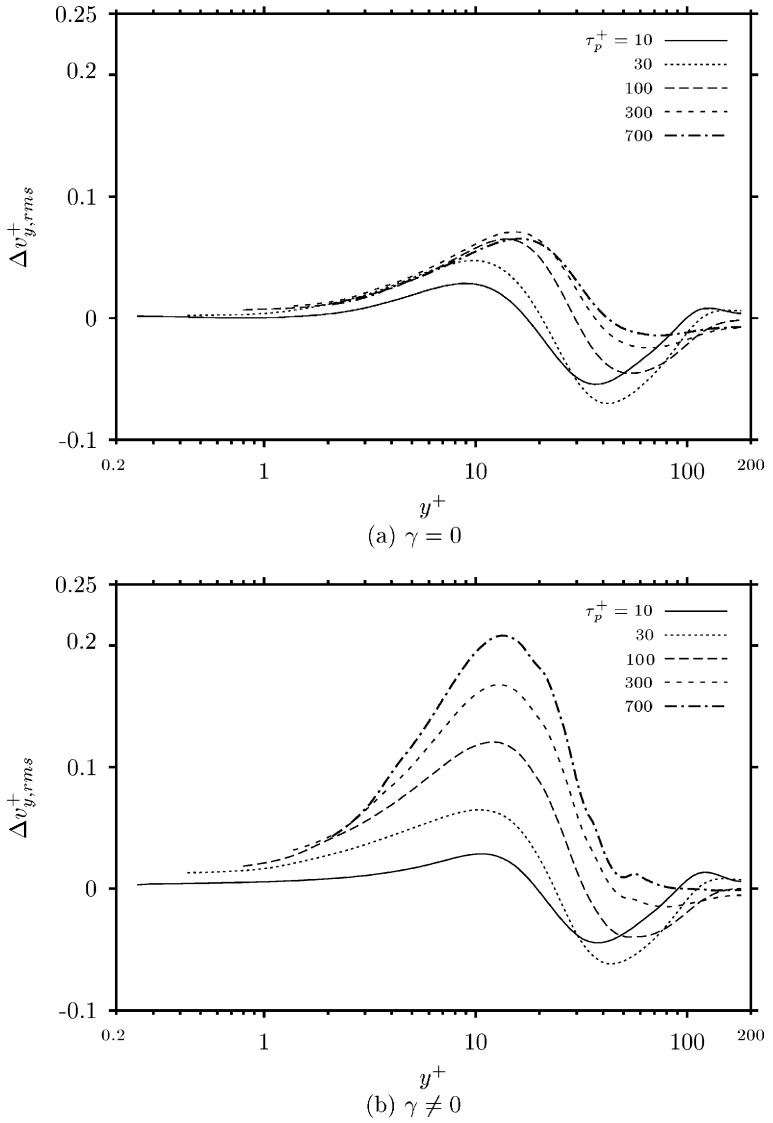

Fig. 4. Distribution of non-equilibrium increment of $v^+_{y,\mathrm{rms}}$ (a) without and (b) with the lift force.

which generates a particle drift toward the wall and therefore plays an important role in the inertial deposition of turbulent particles. Under the assumption that particles are in perfect equilibrium with the local fluid turbulence, the following turbophoretic velocity was defined from Eqs. (5) and (6) (Reeks, 1983; Young and Leeming, 1997):

$$v^+_{\mathrm{t,ep}} = -\frac{24}{Re_\mathrm{p}}\frac{1}{C_\mathrm{D}}\tau_\mathrm{p}\frac{\mathrm{d}}{\mathrm{d}y}\left(\frac{\tau_\mathrm{L}}{\tau_\mathrm{p}+\tau_\mathrm{L}}\langle u_y'^2\rangle\right)\frac{1}{u^*}. \tag{54}$$

Combining Eqs. (9) and (48), the non-equilibrium turbophoretic velocity can be defined in a similar form as Eq. (54), and then it can be decomposed into an equilibrium part, $v_{t,eq}$, and an additional part due to the non-equilibrium memory effect, Δv_t:

$$v_t^+ = v_{t,eq}^+ + \Delta v_t^+, \tag{55}$$

where $v_{t,eq}$ and Δv_t are expressed as, respectively,

$$v_{t,eq}^+ = -\frac{24}{Re_p}\frac{1}{C_D}\tau_p\frac{d}{dy}\left(\zeta_{yy} - D_{yy}\frac{d\bar{v}_y}{dy}\right)\frac{1}{u^*}, \tag{56}$$

$$\Delta v_t^+ = \frac{24}{Re_p}\frac{1}{C_D}\tau_p\frac{d}{dy}\left(\tau_\beta \bar{v}_y\frac{d\zeta_{yy}}{dy}\right)\frac{1}{u^*}. \tag{57}$$

There is a marked discrepancy between the two different equilibrium turbophoretic velocities, $v_{t,ep}$ and $v_{t,eq}$, defined in Eqs. (54) and (56), respectively. The former one $v_{t,ep}$ was derived under the assumption that the particle motion is governed by the Stokes drag force. The equilibrium turbophoretic velocity $v_{t,ep}$ obtained from Eq. (54), therefore, is unrelated with the variation of mean shear rates of both the phases, $s_{f,xy}$ and $s_{p,xy}$. On the other hand, the latter one $v_{t,eq}$ was formulated with the shear-induced lift force acting on the particle motion.

The two equilibrium turbophoretic velocities $v_{t,ep}$ and $v_{t,eq}$ are compared in Fig. 5(a) and (b) for various particle relaxation times. Fig. 5(a) is the case of zero shear-induced lift force ($\gamma = 0$) and Fig. 5(b) the case of non-zero lift force ($\gamma \neq 0$). For comparison with the existing data, the predictions are plotted together with the DNS data from Brooke et al. (1994) for $\tau_p^+ = 3, 5, 10$ where the lift force was not included. Since these particles are small enough to neglect the non-equilibrium memory effects, it will be reasonable to directly compare the DNS results with the equilibrium predictions. The comparison with DNS results clearly shows that the equilibrium turbophoretic velocity calculated from Eq. (56) is in a better agreement than that from Eq. (54).

In the absence of the lift force effect, the existing equilibrium theory tends to predict higher values of turbophoretic velocity than the present theory (Fig. 5(a)). In the existing equilibrium theory, the inclusion of lift force reduces the turbophoresis. The present theory, on the other hand, predicts an increased turbophoresis by the inclusion of lift force. At present there are no experimental data to check the conflicting predictions against, so it remains to be clarified in the future by experiments or Lagrangian particle tracking using DNS or LES.

As mentioned in the preceding section, the particle fluctuating intensity is markedly increased in the near-wall region ($y^+ < 20$) due to the memory effect, and the increased particle turbulence induces an additional turbophoretic velocity, Δv_t. Fig. 6(a) and (b) presents the near-wall distributions of Δv_t^+ as a function of particle relaxation time with and without the lift force effect. As was mentioned in Shin and Lee (2001), the additional turbophoresis due to the non-equilibrium memory effect accelerates the particles toward the wall in the near-wall region ($y^+ < 20$), but in the outer region ($y^+ > 20$) pushes particles away from the wall into the core. This tendency increases with particle relaxation time. In the presence of lift force the additional turbophoretic velocity by non-equilibrium effect is increased by a factor of 2 or 3 over all particle sizes (Fig. 6(b)).

Fig. 7(a) and (b) presents the near-wall distributions of total turbophoretic velocity, v_t, which is the sum of the equilibrium part, $v_{t,eq}$, and the additional part due to the memory effect, Δv_t. When compared with Fig. 5(a) and (b), it is recognized that, due to the non-equilibrium memory effect,

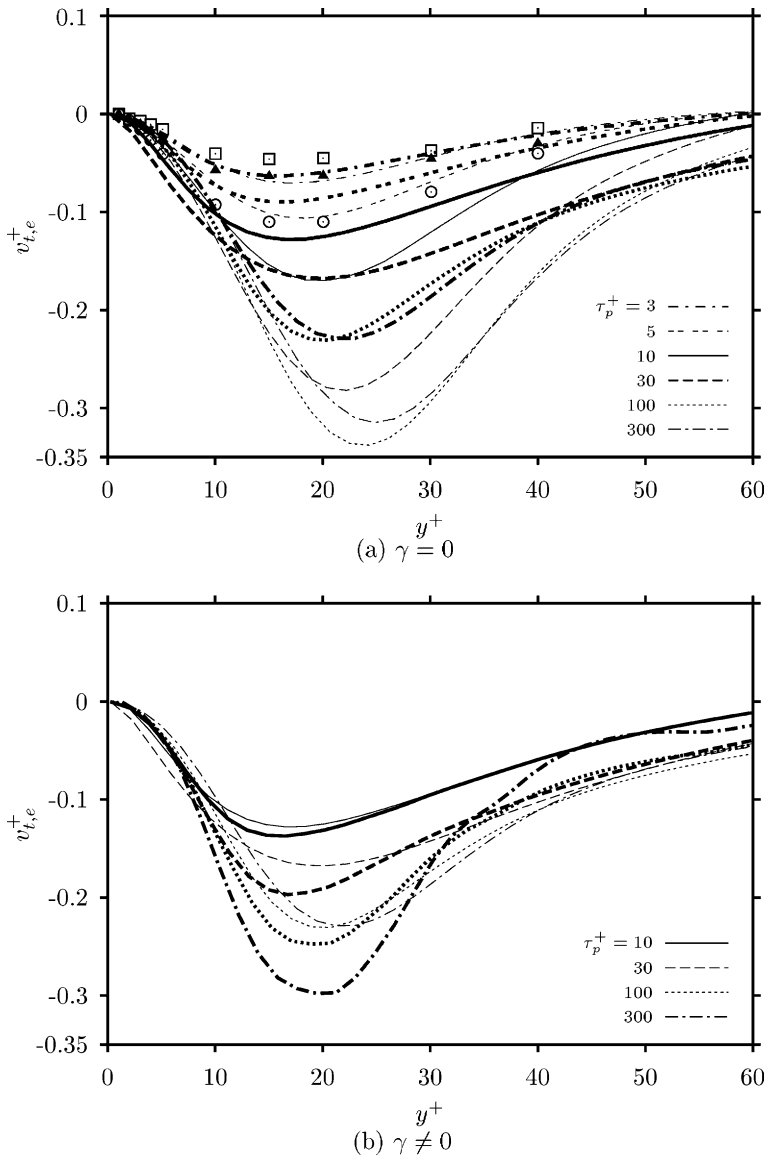

Fig. 5. Distribution of the equilibrium turbophoretic velocity, $v_{t,eq}^+$, (a) without and (b) with the lift force: thin lines, $v_{t,ep}^+$ (existing equilibrium theory); thick lines, $v_{t,eq}^+$ (present theory). DNS data from Brooke et al. (1994): ⊡, $\tau_p^+ = 3$; ▲, $\tau_p^+ = 5$; ⊙, $\tau_p^+ = 10$.

the peak position of the wallward turbophoretic velocity gets closer to the wall than predicted by the existing equilibrium theory. As the particle size increases, the additional part Δv_t contributes more and more to the wallward turbophoretic velocity in the vicinity of the wall ($y^+ < 20$), but it acts in the opposite direction away from the wall in the region of $20 < y^+ < 50$. Thus the profile of the total turbophoretic velocity becomes sharper, taller and closer to the wall with increasing

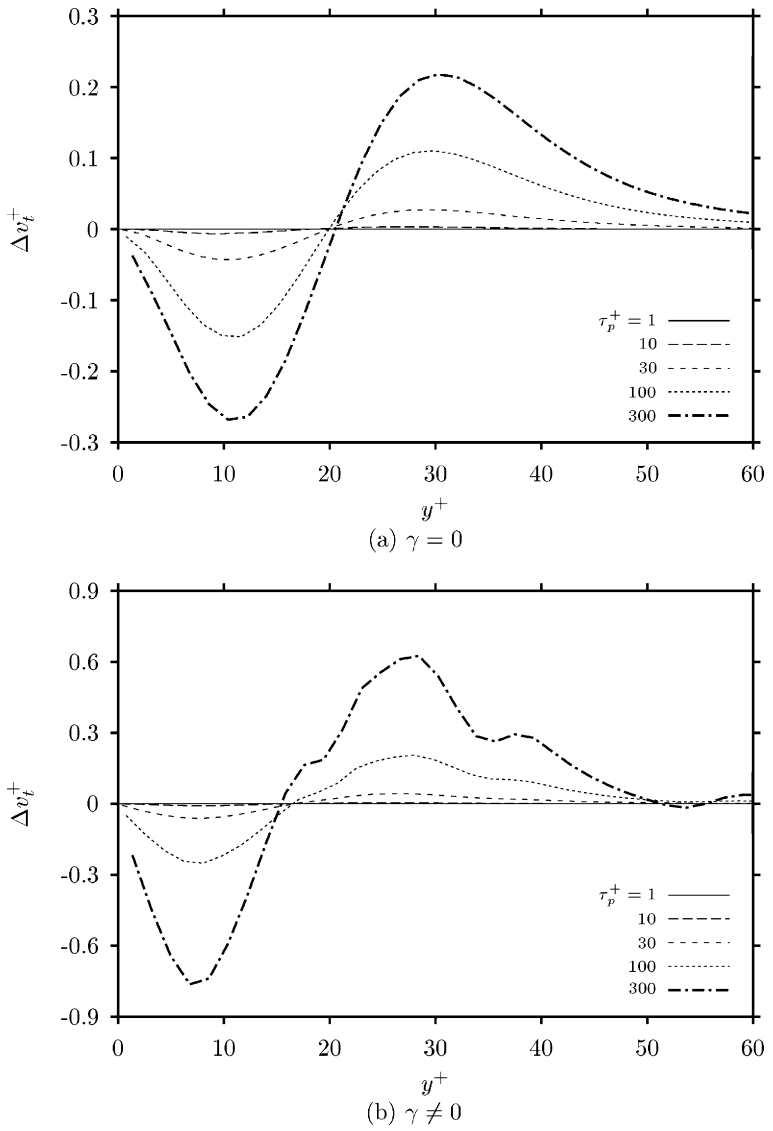

Fig. 6. Distribution of non-equilibrium increment of v_t^+ (a) without and (b) with the lift force.

particle size. This feature of the profile of turbophoretic velocity is unchanged by the inclusion of lift force. The lift force makes the peak position much closer to the wall, and, at the same time, the peak value much higher than in the absence of the lift force.

Fig. 8(a) and (b) shows the peak positions of equilibrium and non-equilibrium turbophoretic velocities as a function of particle relaxation time. For small particles ($\tau_p^+ < 1$), the peak position is located at roughly $y^+ \approx 15$. For larger particles ($\tau_p^+ > 10$), the peak position varies with particle size. The peak position of equilibrium profile $v_{t,eq}$ becomes more distant from the wall with increased particle size. Compared with the results obtained from the present theory, the existing

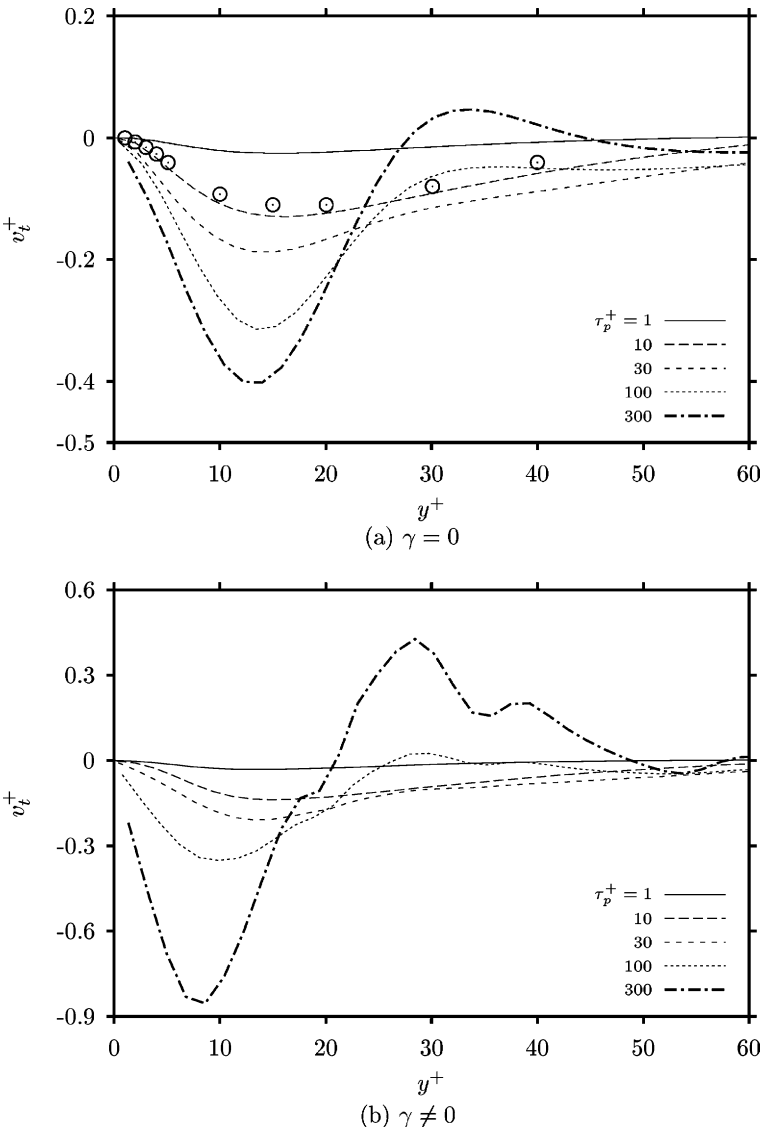

Fig. 7. Near-wall distribution of total turbophoretic velocity (a) without and (b) with the lift force. Symbols, DNS data for $\tau_p^+ = 10$ from Brooke et al. (1994).

equilibrium theory tends to overestimate the variation of peak position with particle size. When the non-equilibrium effect is considered, the peak position changes with particle size in the opposite sense. That is, for moderate or large particles ($\tau_p^+ > 10$), the peak position of v_t gets nearer to the wall with increased particle size. For particles with $\tau_p^+ = 100$, for instance, the existing equilibrium theory predicts the peak position $y_{peak}^+ \approx 24$, but on the other hand the present non-equilibrium theory predicts $y_{peak}^+ \approx 14$ in the absence of the lift force (Fig. 8(a)) and $y_{peak}^+ \approx 11$ in the presence of the lift force (Fig. 8(b)). As is clear from Fig. 8(a) and (b), the inclusion of lift force

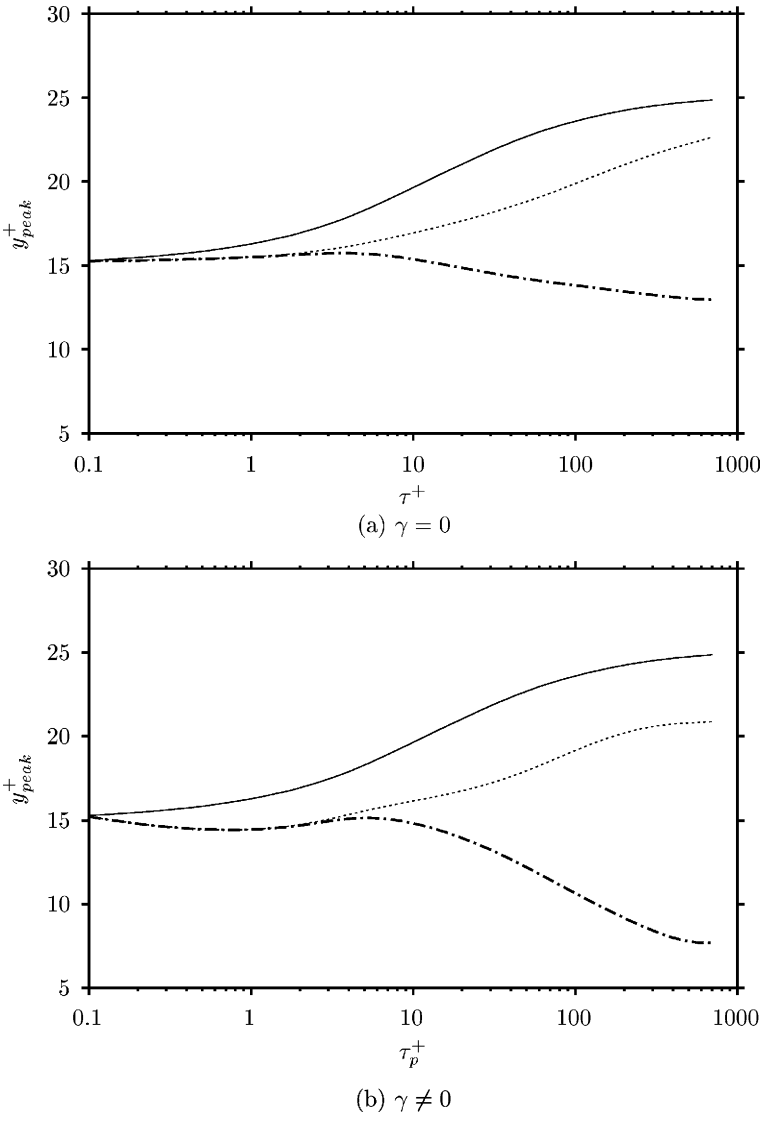

Fig. 8. Predicted change of the peak-position of maximum v_t^+ (a) without and (b) with the lift force: solid line, $v_{t,ep}^+$; dotted lines, $v_{t,eq}^+$; dash-dotted lines, v_t^+.

contributes to moving the peak position of the turbophoretic velocity closer to the wall as well as increasing the peak value.

Though it still needs to be verified in the future, it can be concluded from the above results that, due to the non-equilibrium conditions induced from particle inertia and inhomogeneity of flow turbulence, inertia-dominated particles acquire an additional momentum toward the wall in the near-wall region where the fluid turbulence is too weak to supply the particles with necessary momentum for a free-flight. No existing equilibrium theories have ever provided this mechanism of particle transport inside the turbulent boundary layer. In order to make an agreement with

measured data, for example, the existing free-flight theories introduced various mechanisms giving similar effects in a somewhat ad hoc manner.

4.3. Particle mean velocity

The momentum transport equations (9) and (10) coupled with the constitutive equations (48) and (49) give x-direction and y-direction components of the particle mean velocity. In general, the large particles ($\tau_p^+ > 10$) lead the fluid mainly in the strong shear region ($y^+ < 30$) (Kulick et al., 1994; Rouson et al., 1994). This discrepancy in the streamwise velocities between fluid and particle increases with increasing particle size. Although the transport equations (9) and (10) are not exact but only approximate, the calculation results for the streamwise mean velocity agree well with this general feature in a qualitative sense (Fig. 9(a)). Compared with DNS results (Rouson et al., 1994), the existing equilibrium theory tends to overestimate the relative motion of large particles. This overestimation is seen to be alleviated by considering the non-equilibrium memory effect on the particle Reynolds stress terms. This trend can also be regarded as a supporting evidence for the adequacy of the present formulation. The inclusion of lift force serves to enhance the relative motion of the dispersed phase to the carrier phase (Fig. 9(b)).

Actually v_y plays a key role in the inertial deposition mechanism, and its near-wall distribution is illustrated for several particle sizes ($\tau_p^+ \geqslant 10$) in Fig. 10(a) and (b). The change of $\bar{v}_y$ with particle size is not monotonic. With increasing particle size, $\bar{v}_y$ initially increases in the near-wall region, but begins to decrease beyond certain particle size. This characteristic dependence of $\bar{v}_y$ on particle size is directly related to the roll-off in the deposition velocity, V_{dep}^+, in the inertia-moderated regime ($\tau_p^+ > 30$). When the lift force is not considered, the non-equilibrium situation serves to increase $\bar{v}_y$ restrictively in the near-wall region ($y^+ < 10$) for the particles with $\tau_p^+ < 30$, but, for large particles ($\tau_p^+ > 30$), serves to attenuate the particle velocity over all region of the boundary layer (Fig. 10(a)). The inclusion of the lift force greatly influences the momentum transport of the dispersed phase, enhancing the near-wall wallward velocity by roughly more than 100% of magnitude, and in this case the non-equilibrium situation serves to attenuate the wallward velocity for the particles with $\tau_p^+ > 10$ (Fig. 10(b)).

4.4. Inertial deposition of particles

As is well known, the deposition velocity of inertia-dominated particles decreases with increased particle size beyond a certain limit, resulting in the roll-off in V_{dep}^+. Since this characteristic feature of inertia-dominated particles is related with the non-equilibrium situation, the existing equilibrium theories have never presented a quantitatively acceptable mechanism. This section is devoted to showing the validity of the present theory for presenting a reasonable deposition mechanism and predicting an accurate deposition velocity even in a quantitative sense.

If the particle concentration and the deposition velocity are calculated in the absence of the lift force, it is observed that the effect of particle inertia reduces the build-up of particle concentration (see Fig. 11). As mentioned before in the preceding sections, for moderate-sized particles ($\tau_p^+ = 10$ and 30) the particle RMS velocity and the wallward convective velocity in the vicinity of the wall are higher than those expected by an equilibrium theory due to the non-equilibrium situation

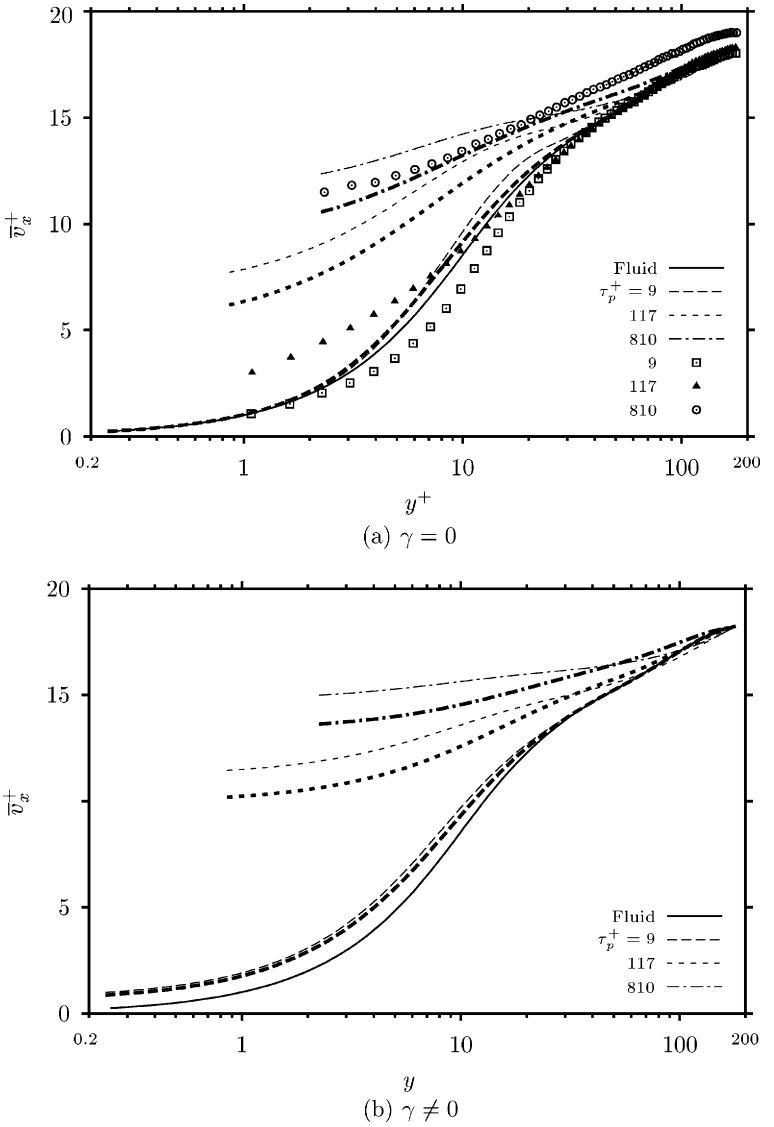

Fig. 9. Distribution of $\overline{v}_x^+$ (a) without and (b) with the lift force: thin lines, equilibrium model; thick lines, non-equilibrium model. DNS data from Rouson et al. (1994): ⊡, 28 μm lycopodium ($\tau_p^+ = 9$); ▲, 50 μm glass ($\tau_p^+ = 117$); ⊙, 70 μm copper ($\tau_p^+ = 810$).

inside the near-wall region. These non-equilibrium mechanisms lead the convective flux of the particles of $\tau_p^+ = 10$ and 30 to increase, resulting in a much reduced concentration level predicted by the equilibrium theory. The predicted non-equilibrium concentration profile in the near-wall region looks reasonable when compared with the DNS results of Brooke et al. (1994). For large particles ($\tau_p^+ > 30$), the concentration profile becomes flat in the near-wall region, which implies that the convective flux is the dominating mechanism in the inertial deposition.

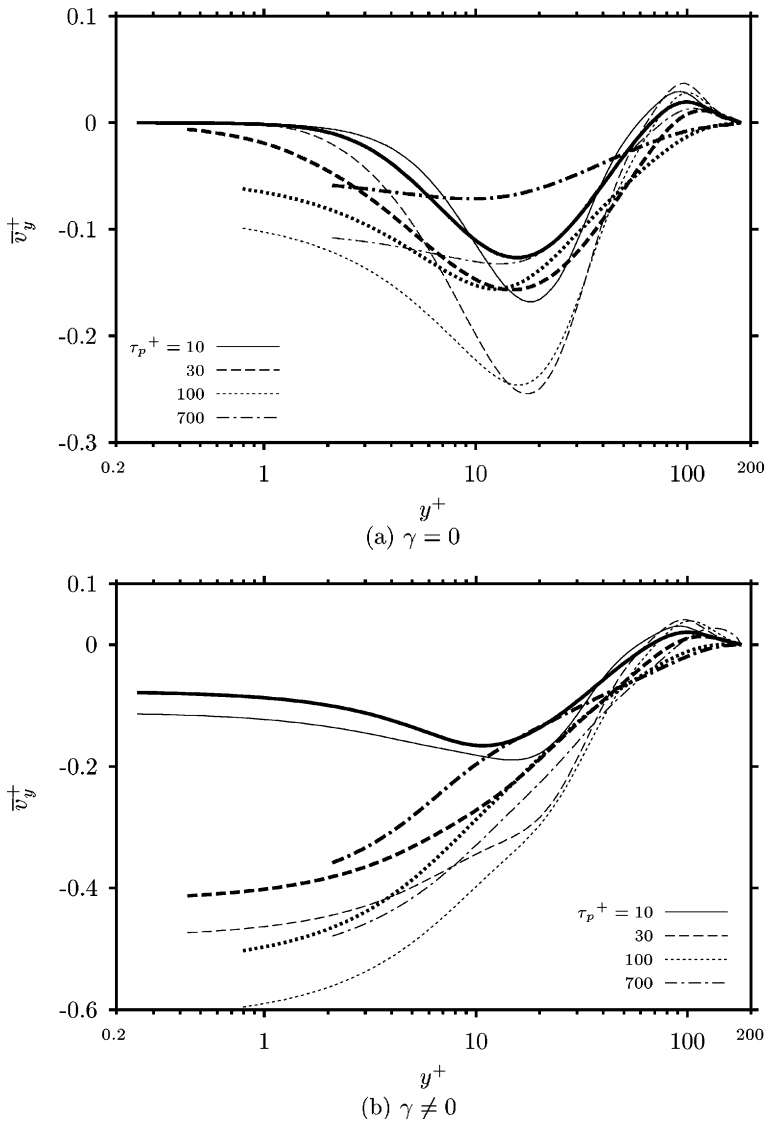

Fig. 10. Distribution of $\bar{v}_y^+$ (a) without and (b) with the lift force: thin lines, equilibrium model; thick lines, non-equilibrium model.

Now the particle deposition velocity, V_{dep}^+, is calculated and compared with the Monte-Carlo simulation of Kallio and Reeks (1989) in Fig. 12. As mentioned before, the non-equilibrium situation in the near-wall region enhances the wallward particle velocity for relatively moderate sized particles ($\tau_{\mathrm{p}}^+ < 30$), but not for large particles ($\tau_{\mathrm{p}}^+ > 30$). Comparison of the predicted deposition velocities with the Lagrangian data implies that the real deposition velocity is higher than the equilibrium prediction in the diffusion–impaction regime ($1 < \tau_{\mathrm{p}}^+ < 30$), but lower in the inertia-moderated regime ($y^+ > 30$). The deposition velocity predicted by the present

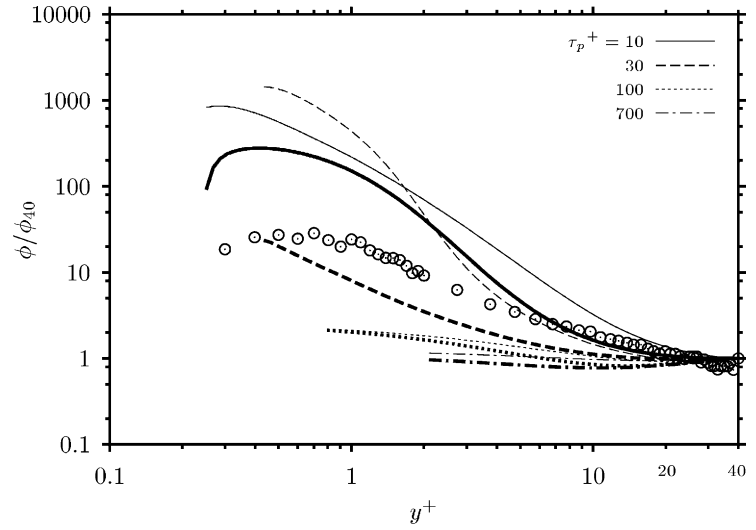

Fig. 11. Concentration profile normalized by ϕ at $y^+ = 40$ in the absence of the lift force: thin lines, Young and Leeming's model; thick lines, present non-equilibrium model; symbols, Brooke et al.'s (1994) data for $\tau_p^+ = 10$.

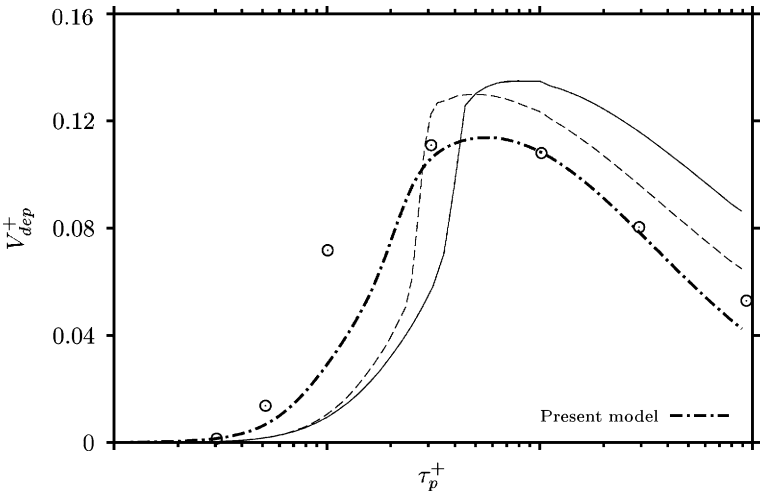

Fig. 12. Predicted deposition velocities as a function of particle relaxation time in the absence of the lift force: solid thin line: Young and Leeming's (1997) model; dashed thin line: Shin and Lee's (2001) model; symbols, Kallio and Reeks (1989).

non-equilibrium model is in excellent agreement with the Lagrangian data even in a quantitative sense. This excellent agreement between the present predictions with the existing Lagrangian simulation data strongly supports the validity of the present non-equilibrium theory.

Now the shear-induced lift force is considered in the deposition process. As mentioned before, the inclusion of the lift force increases the RMS velocity and wallward velocity of the dispersed phase inside near-wall region. Due to these mechanisms, the inclusion of the lift force makes the

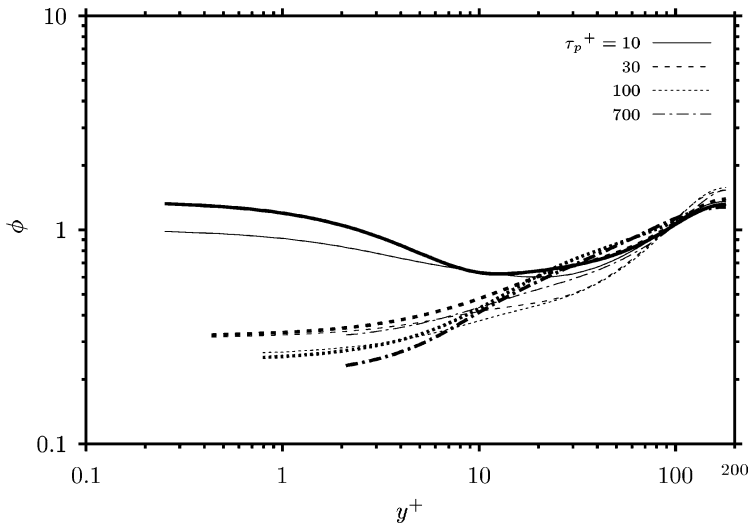

Fig. 13. Concentration profile in the presence of the lift force: thin lines, equilibrium profile; thick lines, non-equilibrium profile.

near-wall profile of particle concentration flat, and the diffusive deposition becomes negligible even for moderate sized particles, $\tau_p^+ \sim O(10)$ (Fig. 13).

Since the lift force is generally thought to increase the deposition velocity, Kallio and Reeks (1989) inferred from their simulation results that the lift force increases the wall-normal particle RMS velocity in the strong shear region, and the increased RMS velocity will lead to an increased particle turbulent diffusivity, which will consequently result in an enhanced deposition. However, this conjecture is not always true. Inside the strong shear region, the inclusion of shear-induced lift force leads to a considerably large drift motion of inertia-dominated particles relative to the carrier fluid, and the relative motion between the two phases may reduce the particle diffusivity due to the effect of crossing trajectories.

On the contrary, when the particle diffusivity is modeled by the dispersion theory of Csanady (1963) (see Eq. (23)), the particle diffusivity for large particles may be remarkably reduced in the near-wall region by the effect of crossing trajectories (Fig. 14). In order to test the effect of crossing trajectories on the deposition velocity, two models are considered in the presence of lift force; one is the case of particle diffusivity equal to the fluid turbulent diffusivity ($\varepsilon_p = \nu_t$), and the other is the case of particle diffusivity modeled by Eq. (23). The deposition velocities calculated with two different diffusivity models are compared in Fig. 15 with existing data (Liu and Agarwal, 1974; Kallio and Reeks, 1989). The existing numerical and experimental data are in good agreement with the predicted deposition velocity using the new diffusivity model which gives reduced particle diffusivity with particle size in the near-wall region.

From this fact, it can be postulated that, in the vicinity of the wall, the shear-induced lift force enhances the convective deposition of inertia-dominated particles through the increased wallward convective velocity, but simultaneously reduces the diffusive deposition of inertia-dominated particles through decreased particle diffusivity. But the enhancement in convective deposition is

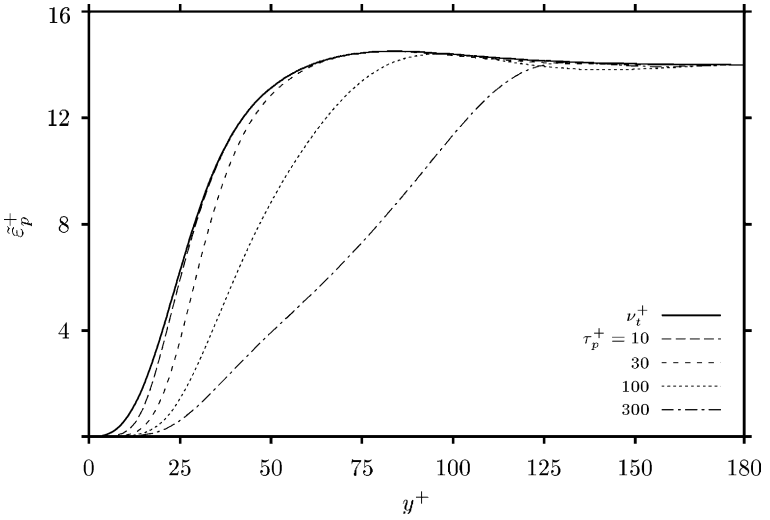

Fig. 14. Dependence of the model diffusivity, $\tilde{\varepsilon}_{\mathrm{p}}^{+}(y^{+})$, on particle inertia.

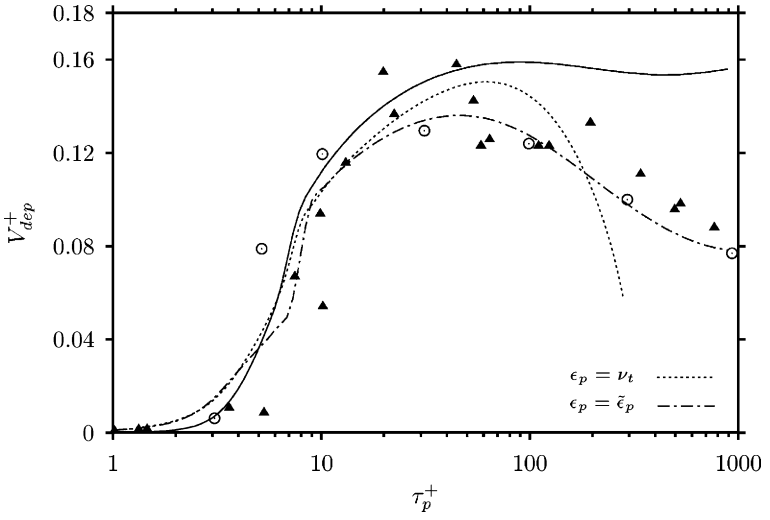

Fig. 15. Predicted deposition velocities with different diffusivity models in the presence of the lift force: solid line, Young and Leeming' model; ⊙, Kallio and Reeks (1989); ▲, Liu and Agarwal (1974).

larger than the reduction in diffusive deposition, so the total deposition velocity of inertia-dominated particles remains higher than that predicted in the absence of the lift force.

Finally, in order to clearly show the validity of the present theory on the non-equilibrium particle Reynolds stress, the predicted deposition velocities are plotted together with the numerically simulated Lagrangian data of Kallio and Reeks (1989), where the two different lift force conditions are considered (Fig. 16). When the lift force is not considered, the particle diffusivity was assumed equal to the fluid turbulent diffusivity over all range of particle sizes ($\varepsilon_{\mathrm{p}}^{+} = \nu_{\mathrm{t}}^{+}$ for all

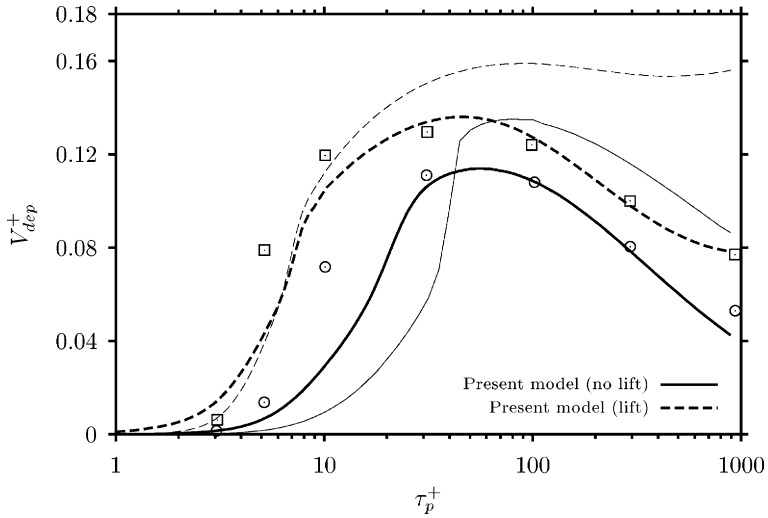

Fig. 16. Comparison of the predicted deposition velocities with the Lagrangian data: solid thin line, Young and Leeming's model (no lift); dotted thin line, Young and Leeming's model (lift); ⊙, Kallio and Reeks (1989, no lift); ⊡, Kallio and Reeks (1989, lift).

τ_p^+), as usual. When the lift force is considered, on the other hand, the effect of crossing trajectories is taken into account in the particle diffusivity for inertia-dominated particles as in the following model:

$$\varepsilon_p^+ = \begin{cases} \nu_t^+ & \text{for } \tau_p^+ < 30, \\ \tilde{\varepsilon}_p^+ & \text{for } \tau_p^+ > 30. \end{cases} \tag{58}$$

For both the cases of with and without lift force included, Eulerian predictions by the present non-equilibrium model are in good agreement with the Lagrangian data.

The unified deposition model was able to predict the inertial deposition of inertia-dominated particles with an improved accuracy by using the present constitutive equations for the particle Reynolds stress accounting for the effects of particle inertia and mean shearing of the carrier flows on the transport of the dispersed phase. But, in order to construct more accurate unified deposition model, a further study is needed on the effects of mean shearing of the fluid phase and the relative drift of the particles to the fluid on the turbulent dispersion of high-inertia particles.

5. Conclusion

In the present study, non-equilibrium mechanism in the transport of inertia-dominated particles was explained in the problem of particle deposition inside a turbulent boundary layer. When the particle relaxation time scale, τ_p, becomes comparable or greater than the characteristic time scale of the system of interest, τ, the particle Reynolds stress is in a non-equilibrium state, and the relaxation time τ_β is then required to reach the equilibrium state. Transport of the inertia-dominated particles is seriously affected also by the mean shearing of the carrier flows. In order to explain such non-equilibrium effects on the transport of the dispersed particle phase, the con-

stitutive equations for the particle Reynolds stress terms were derived from the stochastic differential equation of motion of particles governed not only by the Stokes drag force but also by the shear-induced lift force.

Compared with the traditional Boussinesq approximation and Shin and Lee's (2001) model, the present constitutive model reflects more precisely the dependence of particle Reynolds stress terms on the mean shear rate of the carrier flow as well as the particle inertia. The present constitutive model is different from the traditional ones; that is, the wall-normal stress contains the gradient diffusion term of the wallward particle momentum, the shear stress contains an additional term besides the gradient diffusion term, and so on. In the present work, two kinds of critical assumptions were simply adopted in the formulation due to the lack of any better information; that is, it was assumed that, at first, the near-wall distribution of fluctuating velocities of particles was Gaussian for mathematical simplicity and, at second, the long-time diffusivity of turbulent particle was independent of mean shearing of the carrier flow field.

The present constitutive equations were then applied to the particle Reynolds stress terms in the problem of particle deposition in the fully developed turbulent channel flows. In the deposition predictions, the intermediate diffusion time scale τ was chosen to be close to a characteristic time scale of near-wall turbulent eddies, such as the Lagrangian integral time scale. If τ were chosen to be much larger than τ_p in disregard of near-wall eddy scales, the description of particle transport would have lost information about the non-equilibrium memory effect. The concluding remarks of the present study on the turbulent particle deposition are summarized as follows:

(a) In the near-wall region the wall-normal RMS velocity of the inertia-dominated particles ($\tau_p^+ > 10$) is larger than the equilibrium one, and the discrepancy becomes larger with increased particle size. It can be attributed to the memory effect of large particles by which particles retain a high level of fluctuating intensity as they travel from the turbulent core region into the near-wall region. The inclusion of the shear-induced lift force augments the non-equilibrium increment of the particle RMS velocity with particle inertia.
(b) The non-equilibrium increment of the particle RMS velocity induces an additional turbophoresis, which accelerates the particles toward the wall in the vicinity of the wall, $y^+ < 20$, but in the outer region of $y^+ > 20$ pushes particles away from the wall into the core. Due to this additional non-equilibrium part the peak values of the total turbophoresis are more increased and the peak positions get closer to the wall than those predicted by the equilibrium theory with increasing particle relaxation time. The lift force makes the peak position much closer to the wall and the peak value much higher than in the absence of the lift force.
(c) As the particle relaxation time increases, the non-equilibrium situation serves to increase the wallward particle velocity in the near-wall region for moderate sized particle ($\tau_p^+ < 30$), but for large particles ($\tau_p^+ > 30$) serves to attenuate the particle velocity over all region of the boundary layer. The inclusion of the lift force greatly augments the wallward particle velocity.
(d) Inside the strong shear region of the boundary layer the inclusion of the shear-induced lift force leads to a considerably large drift motion of inertia-dominated particles relative to the surrounding fluid, and the relative motion between the two phases may reduce the turbulent particle diffusivity due to the effect of crossing trajectories.
(e) In the vicinity of the wall the shear-induced lift force not only enhances the convective deposition of inertia-dominated particles through the increased wallward convective velocity but

also simultaneously attenuates the diffusive deposition of inertia-dominated particles through decreased particle diffusivity. The enhancement of convective deposition is larger than the reduction of diffusive deposition, so that the total deposition velocity of inertia-dominated particles remains higher than that predicted in the absence the lift force.

(f) The deposition velocities as a function of particle relaxation time predicted by the present non-equilibrium model are in excellent agreement with existing numerical and experimental data even in a quantitative sense.

Acknowledgement

This work was supported by grant no. 98-0200-03-01-3 from the Basic Research Program of the Korea Science and Engineering Foundation.

Appendix A

A.1. Streamwise mean velocity profile of the carrier phase

The dimensionless velocity profile over a flat plate in the turbulent boundary layer is given as

$$\langle u_1^+ \rangle = \begin{cases} y^+ & \text{for } y^+ \leqslant 5, \\ a_0 + a_1 y^+ + a_2 y^{+^2} + a_3 y^{+^3} & \text{for } 5 < y^+ \leqslant 30, \\ 2.5 \ln y^+ + 5.5 & \text{for } y^+ > 30, \end{cases} \tag{A.1}$$

where $a_0 = -1.076$, $a_1 = 1.445$, $a_2 = -0.04885$, and $a_3 = 0.0005813$ (Kallio and Reeks, 1989).

A.2. Distribution of eddy viscosity inside the boundary layer

The model for the eddy viscosity v_t^+ is a two-layer model where the eddy viscosity for near-wall and core flows are described by two separate functions connected by a smooth transition (Granville, 1990):

$$v_t^+(y^+) = v_c^+ \tanh\left(\frac{v_w^+}{v_c^+}\right). \tag{A.2}$$

In Eq. (A.2), v_c^+ is for the near-wall region, and v_w^+ for the core flow:

$$v_c^+ = 0.4 y^+ \left(1 - \mathrm{e}^{y^{+^2}/24^2}\right), \tag{A.3}$$

$$v_w^+ = 0.03 U_c^+ \delta^+ \left[1.1 - \frac{0.2}{\pi} \tan^{-1}\left(\frac{y^{+2}}{(h^+ - y^+)^2}\right)\right], \tag{A.4}$$

where δ^+ is the momentum thickness:

$$\delta^+ = \int_0^{h^+} \left(1 - \frac{\langle u_1^+ \rangle}{U_c^+}\right) \mathrm{d}y^+, \tag{A.5}$$

where U_c is the mean velocity at the centerline.

A.3. Distribution of fluid RMS velocity inside the boundary layer

The model for the fluid RMS velocity is similar in form to Eq. (A.2) (Young and Leeming, 1997):

$$\sqrt{\langle u_2'^{+2} \rangle}(y^+) = \vartheta_c \tanh\left(\frac{\vartheta_w}{\vartheta_c}\right), \tag{A.6}$$

where

$$\vartheta_c = 0.0373 y^+ \left(1 - \mathrm{e}^{y^+/4.67}\right), \tag{A.7}$$

$$\vartheta_w = 0.9 - \frac{0.54}{\pi} \tan^{-1}\left(\frac{y^{+2}}{(h^+ - y^+)^2}\right). \tag{A.8}$$

In Eqs. (A.7) and (A.8), constants were chosen to satisfy various boundary values and limiting behaviors suggested by the DNS results of Kim et al. (1987).

A.4. Distribution of Lagrangian integral time scale inside the boundary layer

The Lagrangian integral time scale τ_L^+ is given by (Young and Leeming, 1997)

$$\tau_L^+(y^+) = \frac{v_t^+(y^+)}{\sqrt{\langle u_2'^{+2} \rangle}(y^+)}. \tag{A.9}$$

A.5. Empirical formula of the drag coefficient

The drag coefficient is given by the following empirical formula (Serfini, 1954; Sartor, 1975):

$$C_D = \begin{cases} \frac{24}{C_c Re_p} & \text{for } Re_p < 0.1, \\ \frac{24}{Re_p}(1 + 0.0916 Re_p) & \text{for } 0.1 < Re_p < 5.0, \\ \frac{24}{Re_p}(1 + 0.158 Re_p^{2/3}) & \text{for } 5.0 < Re_p < 1000. \end{cases} \tag{A.10}$$

The Cuningham slip correction factor is given by (Hinds, 1982)

$$C_c = 1 + \frac{2}{Pd}(6.32 + 2.01\mathrm{e}^{-0.1095 Pd}), \tag{A.11}$$

where P is the absolute pressure in cm Hg, and d is the particle diameter in μm.

A.6. Evaluation of long-time dispersion coefficients, $\mu_{ij}(\infty)$ and $\lambda_{ij}(\infty)$

The dispersion coefficients are defined as follows (Reeks, 1992):

$$\mu_{ij}(t) = \int_0^t \mathrm{d}s \langle \dot{g}_{ki}(t-s) f'_k(\mathbf{v}, \mathbf{x}, t \,|\, s) f'_j(\mathbf{x}, t) \rangle, \tag{A.12}$$

$$\lambda_{ij}(t) = \int_0^t \mathrm{d}s \langle g_{ki}(t-s) f'_k(\mathbf{v}, \mathbf{x}, t \,|\, s) f'_j(\mathbf{x}, t) \rangle, \tag{A.13}$$

where g_{ki} is the response coefficient satisfying the following equation:

$$\ddot{g}_{ij} = -\dot{g}_{ik} B_{jk} + g_{ik} \frac{\partial \langle f_j \rangle}{\partial x_k} + \delta_{ij} \delta(t). \tag{A.14}$$

g_{ij} denotes the j-directional displacement of the particle due to an impulsive force per unit mass, $\delta(t)$, in the i-direction. Coefficients of **B** and mean aerodynamic forces are given by

$$B_{11} = \beta, \quad B_{12} = 0, \quad B_{21} = \gamma, \quad B_{22} = \beta, \tag{A.15}$$

$$\langle f_1 \rangle = \beta s_\mathrm{f} x_2, \quad \langle f_2 \rangle = \gamma s_\mathrm{f} x_2. \tag{A.16}$$

Then the system of differential equations for the response coefficients is given as follows:

$$\begin{aligned} \ddot{g}_{11} &= -\beta \dot{g}_{11} + \beta s_\mathrm{f} g_{12} + \delta(t), \\ \ddot{g}_{12} &= -\gamma \dot{g}_{11} - \beta \dot{g}_{12} + \gamma s_\mathrm{f} g_{12}, \\ \ddot{g}_{21} &= -\beta \dot{g}_{21} + \beta s_\mathrm{f} g_{22}, \\ \ddot{g}_{22} &= -\gamma \dot{g}_{21} - \beta \dot{g}_{22} + \gamma s_\mathrm{f} g_{22} + \delta(t). \end{aligned} \tag{A.17}$$

From the condition of stationary homogeneous turbulence, the dispersion coefficients $\mu_{ij}(\infty)$ and $\lambda_{ij}(\infty)$ can be reduced to the following simple forms:

$$\mu_{ij}(\infty) = \int_0^\infty \mathrm{d}s \, \dot{g}_{ki}(s) B_{kn} B_{jm} Q_{nm}(s), \tag{A.18}$$

$$\lambda_{ij}(\infty) = \int_0^\infty \mathrm{d}s \, g_{ki}(s) B_{kn} B_{jm} Q_{nm}(s), \tag{A.19}$$

where $Q_{nm}(s)$ is the Lagrangian autocorrelation function of the carrier turbulence. In general, it is not expected that a universal form exists for the correlation function of homogeneous turbulence. As usual it can be approximated with an exponential form on the ground of mathematical simplicity (Hinze, 1975; Reeks, 1992):

$$Q_{nm}(s) \approx \langle u'_n u'_m \rangle \mathrm{e}^{-s/\tau_{\mathrm{L},nm}}, \tag{A.20}$$

where $\tau_{\mathrm{L},nm}$ is a Lagrangian integral time scale associated with the autocorrelation of fluid velocities $\langle u'_n(0) u'_m(s) \rangle$.

References

Beal, S.K., 1968. Deposition of particles in turbulent flow on channel or pipe wall. Nucl. Sci. Eng. 40, 1–11.
Brodkey, R.S., Wallace, J.M., Eckelmann, H., 1974. Some properties of truncated turbulence signals in bounded shear flows. J. Fluid Mech. 63, 209–224.
Brooke, J.W., Hanratty, T.J., McLaughlin, J.B., 1994. Free-flight mixing and deposition of aerosols. Phys. Fluids 6, 3404–3415.
Csanady, G.T., 1963. Turbulent diffusion of heavy particles in the atmosphere. J. Atmos. Sci. 20, 201–208.
Chao, B.T., 1964. Turbulent transport behaviour of small particles in dilute suspension. Osterr. Ing. Arch. 18, 7–21.
Davies, C.N. (Ed.), 1966. Deposition from Moving Aerosols. In: Aerosol Science. Academic Press, London.
Friedlander, S.K., 1957. Behavior of suspended particles in a turbulent fluid. AIChE 3, 381–385.
Friedlander, S.K., Johnstone, H.F., 1957. Deposition of suspended particles form turbulent gas streams. Ind. Eng. Chem. 49, 1151–1156.
Granville, P.S., 1990. A near-wall eddy viscosity formula for turbulent boundary layers in pressure gradients suitable for momentum, heat, or mass transfer. Trans. ASME: J. Fluids Eng. 112, 240–243.
Guha, A., 1997. A unified Eulerian theory of turbulent deposition to smooth and rough surfaces. J. Aerosol Sci. 28, 1517–1537.
Hinds, W.C., 1982. Aerosol Technology. Wiley, New York.
Hinze, J.O., 1975. Turbulence. In: Mechanical Engineering. McGraw-Hill, New York.
Kallio, G.A., Reeks, M.W., 1989. A numerical simulation of particle deposition in turbulent boundary layers. Int. J. Multiphase Flow 15, 433–446.
Kim, J., Moin, P., Moser, R., 1987. Turbulence statistics in fully developed channel flow at low Reynolds number. J. Fluid Mech. 177, 133–166.
Kulick, J.D., Fessler, J.R., Eaton, J.K., 1994. Particle response and turbulence modification in fully-developed channel flow. J. Fluid Mech. 277, 109–134.
Liu, B.Y., Ilori, T.Y., 1974. Aerosol deposition in turbulent pipe flow. Environ. Sci. Tech. 8, 351–356.
Liu, B.Y., Agarwal, J.K., 1974. Experimental observation of aerosol deposition in turbulent flows. J. Aerosol Sci. 5, 145–155.
Luchik, T.S., Tiederman, W.G., 1987. Timescale and structure of ejections and bursts in turbulent channel flows. J. Fliud Mech. 174, 529–552.
Meek, C.C., Jones, B.G., 1974. Studies on the behavior of heavy particles in a turbulent fluid flow. J. Atmos. Sci. 30, 239–244.
Papavergos, P.G., Hedley, A.B., 1984. Particle deposition behaviour from turbulent flows. Chem. Eng. Res. Des. 62, 275–295.
Peskin, R.L., 1971. Stochastic Estimation Applications to Turbulent Diffusion. In: Chiu, C.L. (Ed.), International Symposium on Stochastic Hydraulics. University of Pittsburgh, Pittsburgh, pp. 251–267.
Pismen, L.M., Nir, A., 1978. On the motion of suspended particles in stationary homogeneous turbulence. J. Fliud Mech. 84, 193–206.
Reeks, M.W., Skyrme, G., 1976. The dependence of particle deposition velocity on particle inertia in turbulent pipe flow. J. Aerosol Sci. 7, 485–495.
Reeks, M.W., 1977. On the dispersion of small particles suspended in an isotropic turbulent field. J. Fluid Mech. 83, 529–546.
Reeks, M.W., 1982. COPDIRC—calculation of particle deposition in reactor coolants. CEGB Report TPRD/B/0016/N82.
Reeks, M.W., 1983. The transport of discrete particles in inhomogeneous turbulence. J. Aerosol Sci. 14, 729–739.
Reeks, M.W., 1992. On the continuum equations for dispersed particles in non-uniform flows. Phys. Fluids A 4, 1290–1303.
Reeks, M.W., 1993. On the constitutive relations for dispersed particles in non-uniform flows, I: Dispersion in a simple shear flow. Phys. Fluids A 5, 750–761.
Rouson, D.W.I., Eaton, J.K., Abrahamson, S.D., 1994. A direct numerical simulation of a particle-laden turbulent channel flow. Report No. TSD-101, Stanford University.

Saffman, P.G., 1965. The lift on a small sphere in a slow shear flow. J. Fluid Mech. 22, 385–400.
Sartor, J.D., 1975. Prediction and measurement of the accelerated motion of water drops in air. J. Appl. Meteorol. 14, 232–239.
Serfini, J.S., 1954. Impingement of water droplets on wedges and double-wedge airfoils at supersonic speeds. NACA Report, 1159.
Shin, M., Lee, J.W., 2001. Memory effect in the Eulerian particle deposition in a fully developed turbulent channel flow. J. Aerosol Sci. 32, 675–693.
Tchen, C.M., 1947. Mean value and correlation problems connected with the motion of small particles suspended in a turbulent fluid. Ph.D. thesis, University of Delft.
Wallace, J.M., Eckelmann, H., Brodkey, R.S., 1972. The wall region in turbulent shear flows. J. Fluid Mech. 54, 39–48.
Young, J.B., Leeming, A.D., 1997. A theory of particle deposition in turbulent pipe flow. J. Fluid Mech. 340, 129–159.